UCID- 17560

Lawrence Livermore Laboratory

Electrostatic Direct Energy Converter
Performance and Cost Scaling Laws

Myron A. Hoffman

August 1977

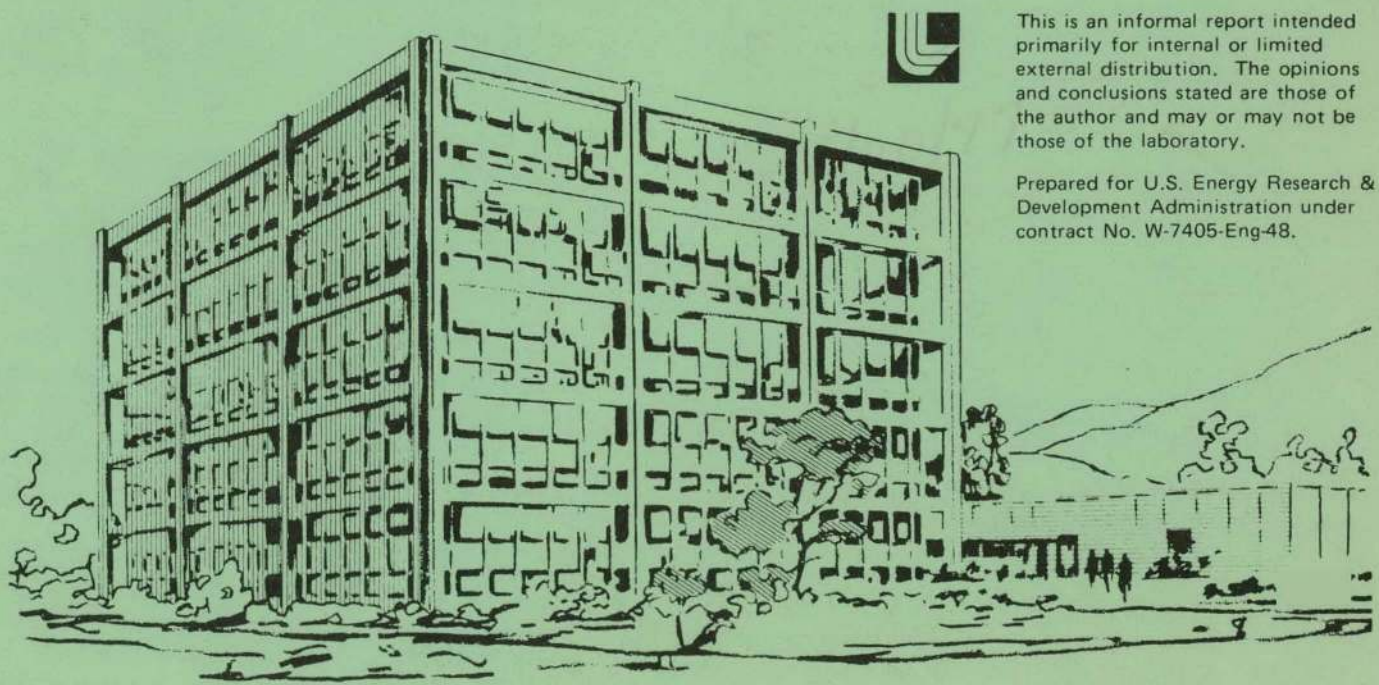

Prepared for U.S. Energy Research & Development Administration under contract No. W-7405-Eng-48.

DISCLAIMER

Electrostatic Direct Energy Converter

Performance and Cost Scaling Laws

Myron A. Hoffman

June 24, 1977

ABSTRACT

This study is concerned with electrostatic type direct energy converters for direct recovery of a large fraction of the plasma ion energy from fusion reactors. Simplified equations are presented for each of the important loss mechanisms in both single-stage direct converters and multistage "Venetian Blind" type direct converters. These equations can be used to estimate the efficiency and electric power output of the direct converter subsystem. Scaling relations for the cost of each major component in the direct converter subsystem are also given; these include the vacuum tank, direct converter modules, the DC power conditioning equipment, cryogenic vacuum pumping system, and the thermal bottoming plant. The performance and cost scaling laws have been developed primarily for use in overall fusion power plant systems codes. However, to illustrate their utility, cost-effectiveness studies of two specific reference direct converter designs are presented in terms of the specific capital costs (i.e., the capital cost per unit electric power produced) for the Direct Converter Subsystem alone. Some examples of design improvements which can significantly reduce the specific capital costs of the Direct Converter Subsystem are also given.

Table of Contents

NOMENCLATURE

A	area (m^2)
$\hat{A}_{RD}$	Richardson-Dushman constant
C	cost (dollars)
$\tilde{C}$	specific costs (dollars per various units)
e	electron charge (coulombs)
ER	expansion ratio
f	fraction (dimensionless)
f_I	leakage ion energy distribution function (dimensionless)
H	height (m)
I	current (amperes)
j	current density (A/m^2)
k	Boltzmann constant
K, k	empirical constants
$K_{B(EFF)}$	effective baffle conductance ratio
L	length (m)
m	empirical exponent
$\bar{M}$	average molecular weight of D_2 and T_2
MPR	mirror power reactor
n_o	background neutral D_2 and T_2 gas density (m^{-3})
P	power (kW)
PS	possible substitute
$\dot{Q}_{TOT}$	total thermal power flow into the cryogenic refrigerators (kW)
q''	heat flux (W/m^2)

R	radius
$R_{M(PL)}$	mirror ratio with plasma present
SCC	specific capital costs ($/kW$_e$)
SGC	specific generating costs (mills/kW-hr)
SF	safety factor
SS, SSDC	single stage direct converter
T	temperature (K)
t	time (seconds)
V	voltage (kV)
VB, VBDC	venetian blind direct converter
W	particle energy (keV)
α_o	ion beam angle of incidence at entrance to the first collector stage
α_i	angle of the ith collector plates
γ	secondary electron emission coefficient
δ	thickness (m)
ε	emissivity
η	efficiency
Θ	angle
ϕ_w	work function (V)
σ	Stefan-Boltzmann constant
σ_{cx}	cross-section for charge exchange (m^2)

Subscripts

a	atmospheric
BFF	B field fan
BOTT	thermal bottoming plant
BT	Burleigh type vacuum tank
C	collector

Ci	ith collector
COMB	combined direct converter and thermal bottoming plant
CP	cryopanels
CR	cryogenic refrigerators
CX, CXL	charge exchange (loss)
DC	direct converter
DCM	direct converter modules
DCS	direct converter subsystem
DT	deuterium and tritium
E	electric
e	electrons
EFF	effective
Gi, Gj	ith or jth current group
GG	grounded grid
I	ions
ID	ideal
INC	incident
INT	interception
k	kth component efficiency loss
M	at the mirror point
N, NG	negative grid
NI	nuclear island
NU	nonuniform spatial distribution
O	at the plasma center
OP	operating costs
PC	power conditioning equipment
PP	pumping power
R	refrigerator

s	sticking
SAI	spread in angle of incidence
SEC	secondary emission
SGi	ith suppressor grid
ST	structural support members
T	tank
TEM	thermionic emission
TH	thermal
TOT	total
TP	thermal panels
TT	thin-walled tank

Electrostatic Direct Energy Converter

Performance and Cost Scaling Laws

Myron A. Hoffman

1. Objectives

This study of electrostatic direct energy converters for the leakage ions from fusion reactors was performed with two objectives in mind:

(1) to develop a set of relatively simple performance and cost equations which accurately model direct converters for use in overall fusion power plant systems codes.

(2) to perform some interesting trade off and "suboptimization" studies on two specific direct converter designs (and also to test the utility and self-consistency of the equations).

The experimental progress on electrostatic DC's (Direct Converters) has been impressive (see, for example, Refs. [1] to [3]) and has led to a series of conceptual design studies of full scale direct converters for future magnetic fusion power plants.

The basic elements of a typical DC Subsystem are shown in Fig. 1. In order to evaluate the cost-effectiveness of DC's in fusion powerplant system studies such as described in Ref. [4], it is necessary to have equations for the electric power produced in the DC, $P_{E(DC)}$, and in the bottoming plant, $P_{E(BOTT)}$, as well as the efficiency of the DC Subsystem, η_{COMB}, and its cost, C_{DCS}. (See App. A for further details). In this report, equations and scaling laws are presented for estimating these parameters. The combined DC plus bottoming plant efficiency is defined as:

$$\eta_{COMB} \equiv \frac{P_{E(DCS)}}{P_{TOT(M)}} = \frac{P_{E(DC)} + P_{E(BOTT)} - P_{E(VPS)}}{P_{TOT(M)}}$$

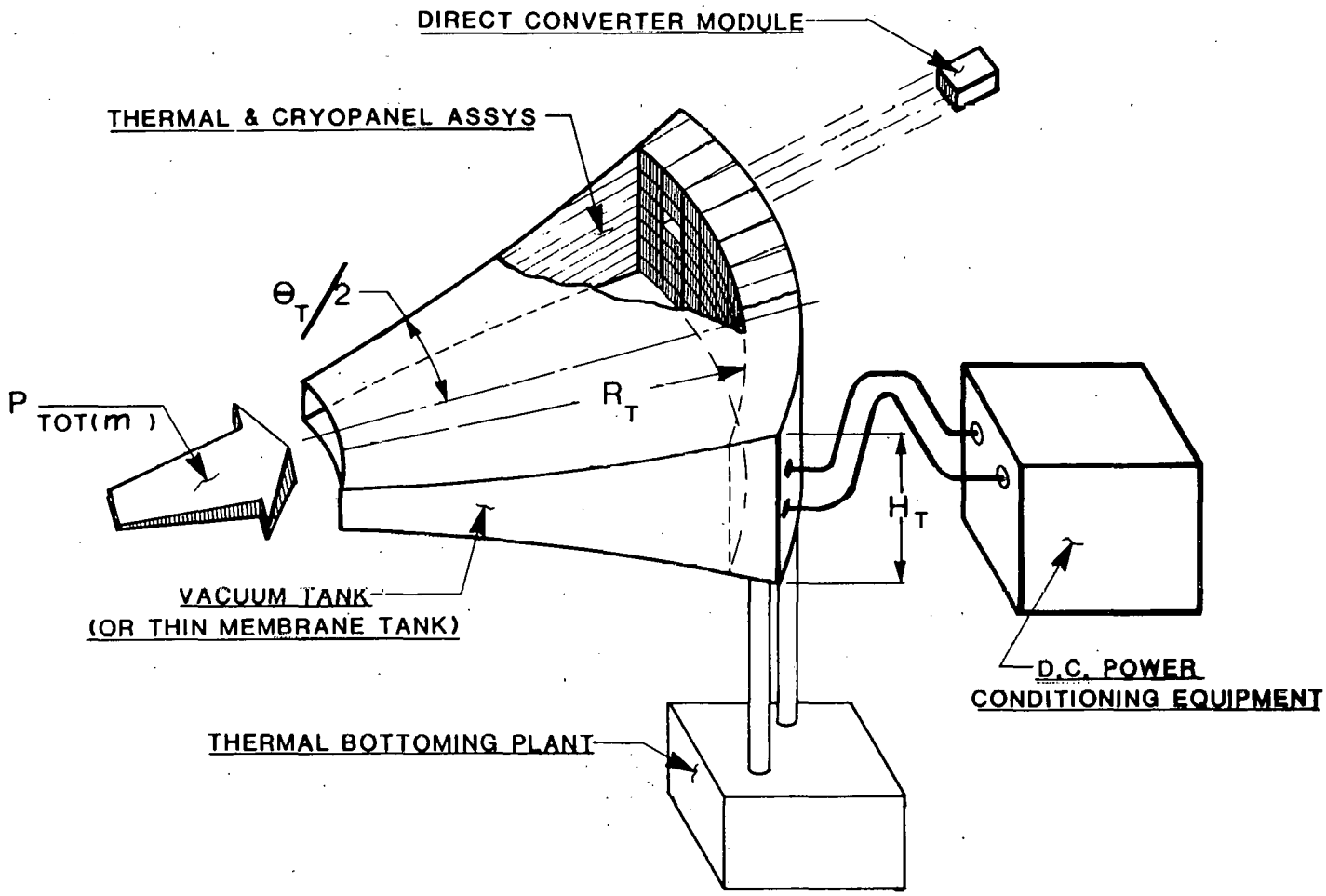

Fig. 1 Major components of the Direct Converter Subsystem (DCS).

where $P_{E(DC)}$ is the electric power from the direct convertors, $P_{E(BOTT)}$ is the additional electric power generated by the thermal bottoming plant associated with the DC Subsystem, $P_{E(VPS)}$ is the power for the vacuum pumping system and $P_{TOT(M)}$ is the total mirror leakage power which goes to the DC Subsystem. The vacuum pumping power is typically only 1 to 2% of the DCS electric power output, and has not been charged against the DCS in this study.

The basic principles of operation of electrostatic direct converters have been described in detail in several papers including Refs. [5] to [11] and will not be repeated here. Suffice it to say that the process of direct conversion of the kinetic energy of the leakage plasma ions to electric energy involves the following processes:

1) Expansion of the leakage particles along magnetic field lines to convert most of the gyro motion to directed kinetic energy.

2) Separation and collection of the electrons on a grounded grid.

3) Electrostatic deceleration of the ions by electrodes maintained at appropriate voltages.

4) Collection of the ions on these collector electrodes.

In this report, specific numerical examples are also given for two types of electrostatic Direct Converters (DC's) for which reference designs were available from the 1976 pure fusion Mirror Power Reactor (MPR) design [5] shown in Fig. 2. The first is a single-stage direct converter (SSDC) which handles 20% of the leakage power, and the second is a three-stage venetian blind direct converter (VBDC) which handles the remaining 80%. Typical modules for these two DC designs are shown in Fig. 3. These designs incorporate the experience gained on the previous design studies of Refs. [6] to [9], as well as the detailed models for each of the loss mechanisms in these types of direct converters developed in Refs. [10] to [14]. In these DC designs it has been assumed that there

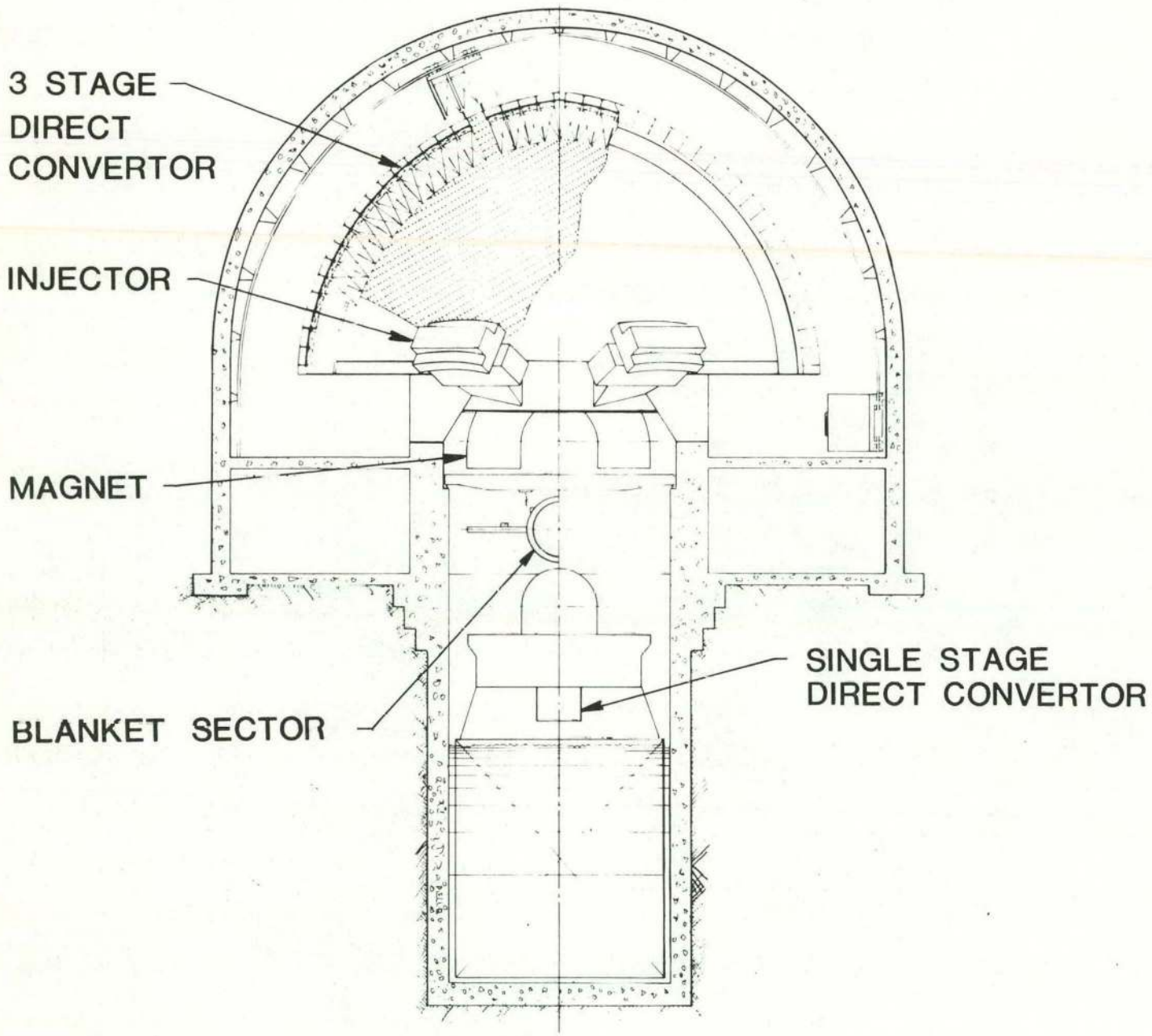

Fig. 2 Pure fusion, Mirror Power Reactor (MPR) conceptual design study of Ref. [5].

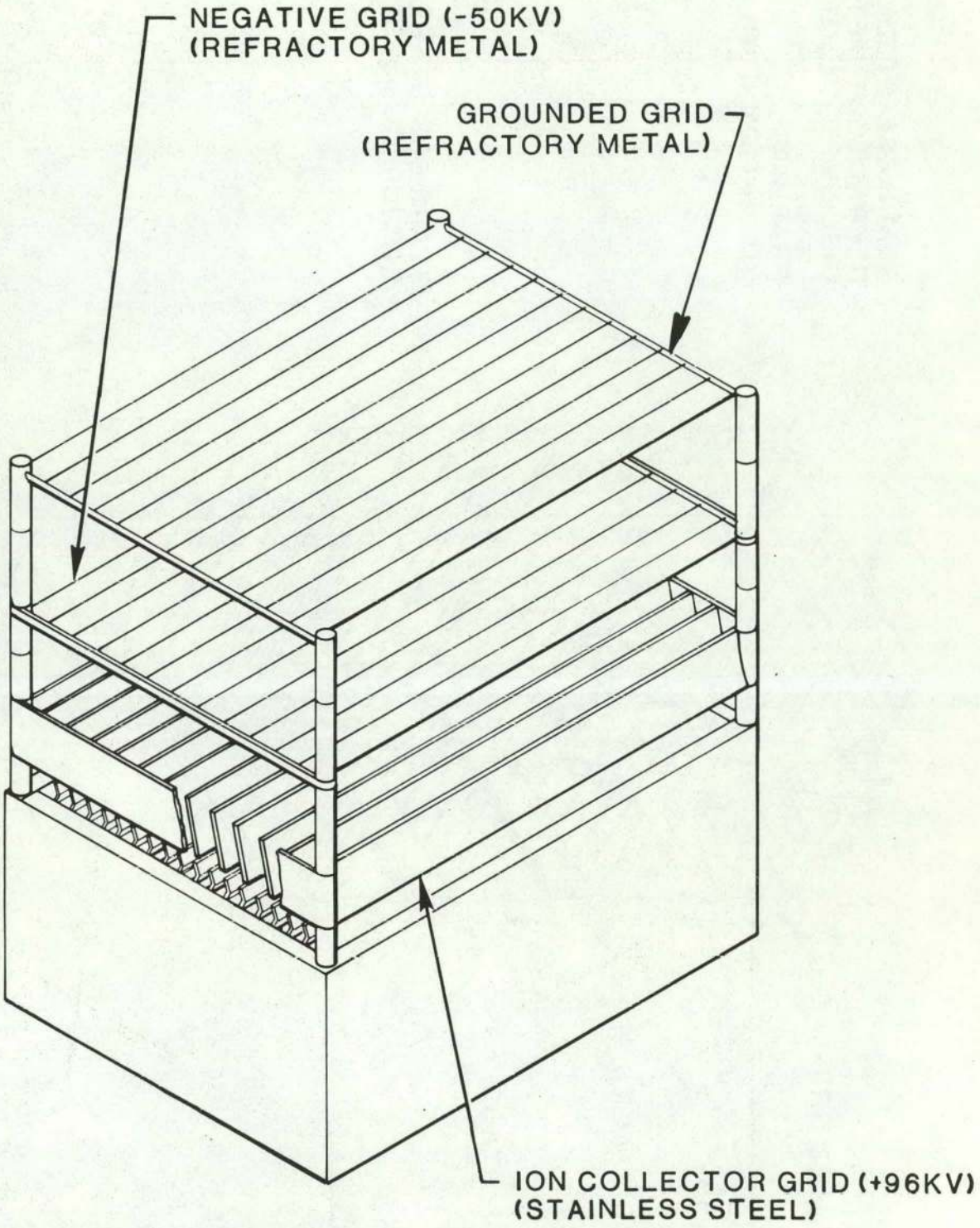

Fig. 3a Reference Single Stage Direct Converter (SSDC) of Ref. [5].

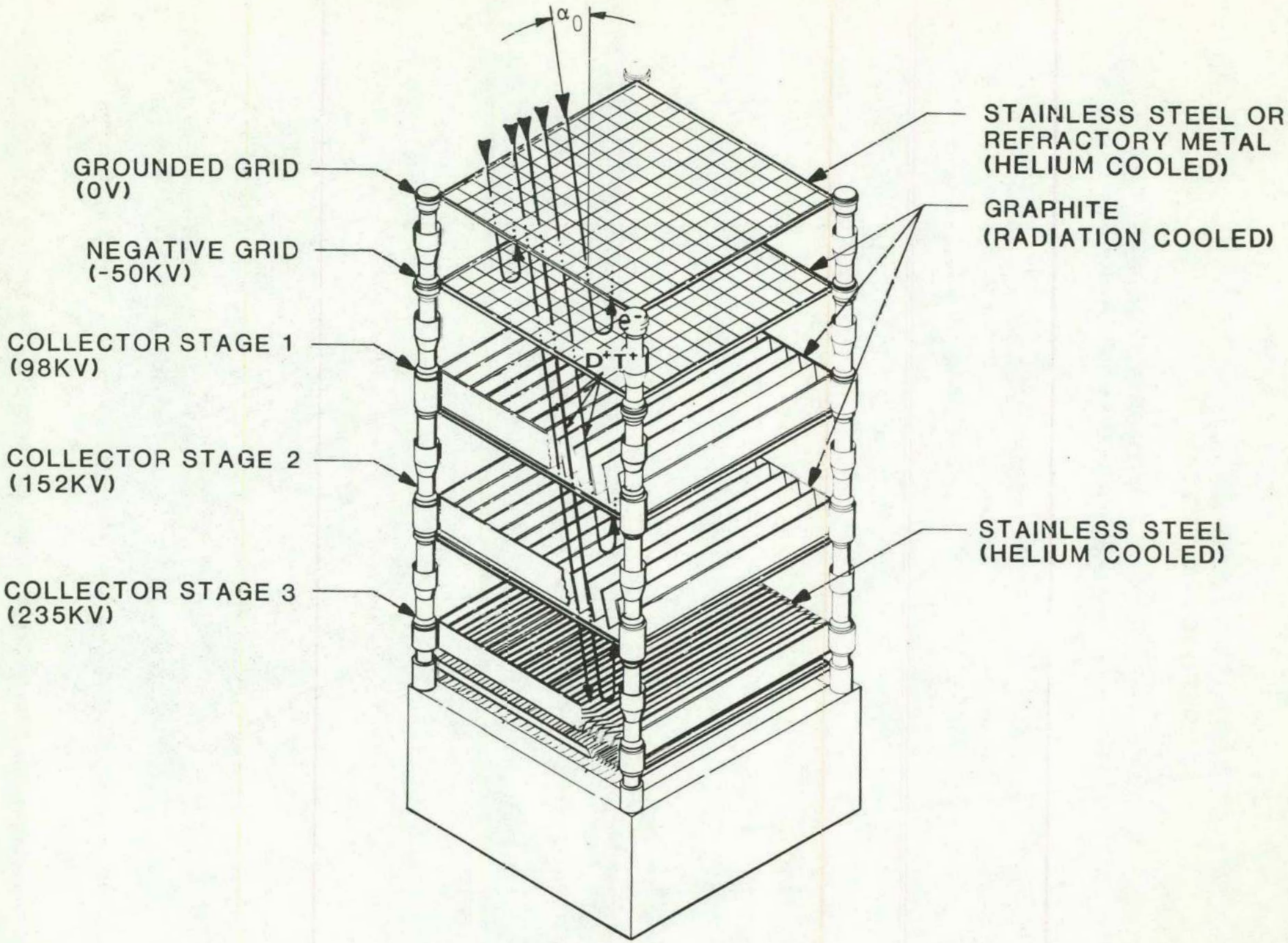

Fig. 3b Reference three-stage Venetian Blind Direct Converter (VBDC) of Ref. [5].

is no selective leakage so that all the mirror leakage charged particle flow comes out a single mirror exit for each of the direct converters and is expanded in the natural fringe field of the magnetic coils. However, the modifications in the equations and scaling laws to include selective leakage or expansion in modified magnetic expanders are not particularly difficult.

The scaling laws presented can be used to examine the effect on the performance of the reference DC designs of changes in the power flux to the direct converter modules, changes in background neutral gas pressure in the expander tank, certain changes in structural materials and structural concepts, etc. However, it should be noted that the equations cannot be used to design a new direct converter significantly different from the reference DC designs, since for simplicity we have chosen to input many parameters which are tied to these specific reference designs. In particular, the grid wire and collector plate dimensions have already been selected to meet the various physics constraints of space charge limits, field emission limits, electric field uniformity, no retrograde ions, and so forth.

2. SSDC Efficiency Estimation

The direct converter efficiency can be written

$$\eta_{DC} \equiv \frac{P_{E(DC)}}{P_{TOT(M)}} = \frac{P_{E(DC)}}{P_{I(M)} + P_{e(M)}}$$

where $P_{I(M)}$ is the ion power flow and $P_{e(M)}$ is the electron power flow out the mirror. We define the fraction of the total mirror leakage power carried by electrons as:

$$f_e = \frac{P_{e(M)}}{P_{TOT(M)}} = 1 - \frac{P_{I(M)}}{P_{TOT(M)}}$$

Further, we assume that the alpha particle power is included in the ion power flow for those cases where the alpha particles transfer most of their energy to the D^+ and T^+ ions and are essentially thermalized. This simplification of including the alphas with the other ions is valid as long as the burn fractions remain low.

The electric power generated in the DC can be related to the mirror leakage power by

$$P_{E(DC)} = P_{TOT(M)} - P_e - \Delta P_{CX} - \Delta P_{GG} - \Delta P_{NG} - \Delta P_{ST} - \Delta P_C$$

where the power loss terms are defined as follows:

- ΔP_{CX} is the power loss due to charge exchange (CX) of the ions with the background D_2 and T_2 molecules
- ΔP_{GG} is the power loss due to ion interception by the grounded grid (GG)
- ΔP_{NG} is the power loss due to interception (INT), thermionic emission (TEM) and secondary emission (SEC) losses from the negative grid (NG) including power supply drains.

ΔP_{ST} is the power loss due to interception on any additional structural members used to support the DC assembly or modules

ΔP_C in an SSDC is the power loss due to the collection of the ions at a single potential and at a finite expansion ratio, ER_C.

Using those definitions the SSDC efficiency can be written:

$$\eta_{SSDC} = 1 - f_e - \Delta\eta_{CX} - \Delta\eta_{GG} - \Delta\eta_{NG} - \Delta\eta_{ST} - \Delta\eta_C$$

$$= (1 - f_e)[1 - \Delta\eta'_{CX} - \Delta\eta'_{GG} - \Delta\eta'_{NG} - \Delta\eta'_{ST} - \Delta\eta'_C] \quad (1A)$$

where each $\Delta\eta$ is defined as:

$$\Delta\eta_k = \frac{\Delta P_k}{P_{TOT(M)}} \quad ; \quad \Delta\eta'_k = \frac{\Delta P_k}{P_{I(M)}} = \frac{\Delta\eta_k}{(1 - f_e)} \quad (1B)$$

(The various losses are illustrated schematically in Fig. 4 including those for a 3-stage VBDC.) It should be noted that the above non-dimensional formulation has the advantage that the losses can be calculated <u>in any order desired</u> once the appropriate loss fractions for each process are specified. The expression of the $\Delta\eta$'s in terms of these loss fractions will be given next.

The loss in efficiency due to charge exchange occurs primarily in the expander region (see Figs. 1 and 2) and can be written simply as:

$$\Delta\eta'_{CX} = f_{CXL} \quad (2)$$

The fractional charge exchange loss from the ion beam, f_{CXL}, is defined as

$$f_{CXL} \equiv \frac{\Delta I_{CXL}}{I_{I(M)}} = 1 - e^{-(n_o \bar{\sigma}_{CX} L_{EX})} \quad (3)$$

$$\approx n_o \bar{\sigma}_{CX} L_{EX} \quad (\text{for } f_{CXL} \ll 1)$$

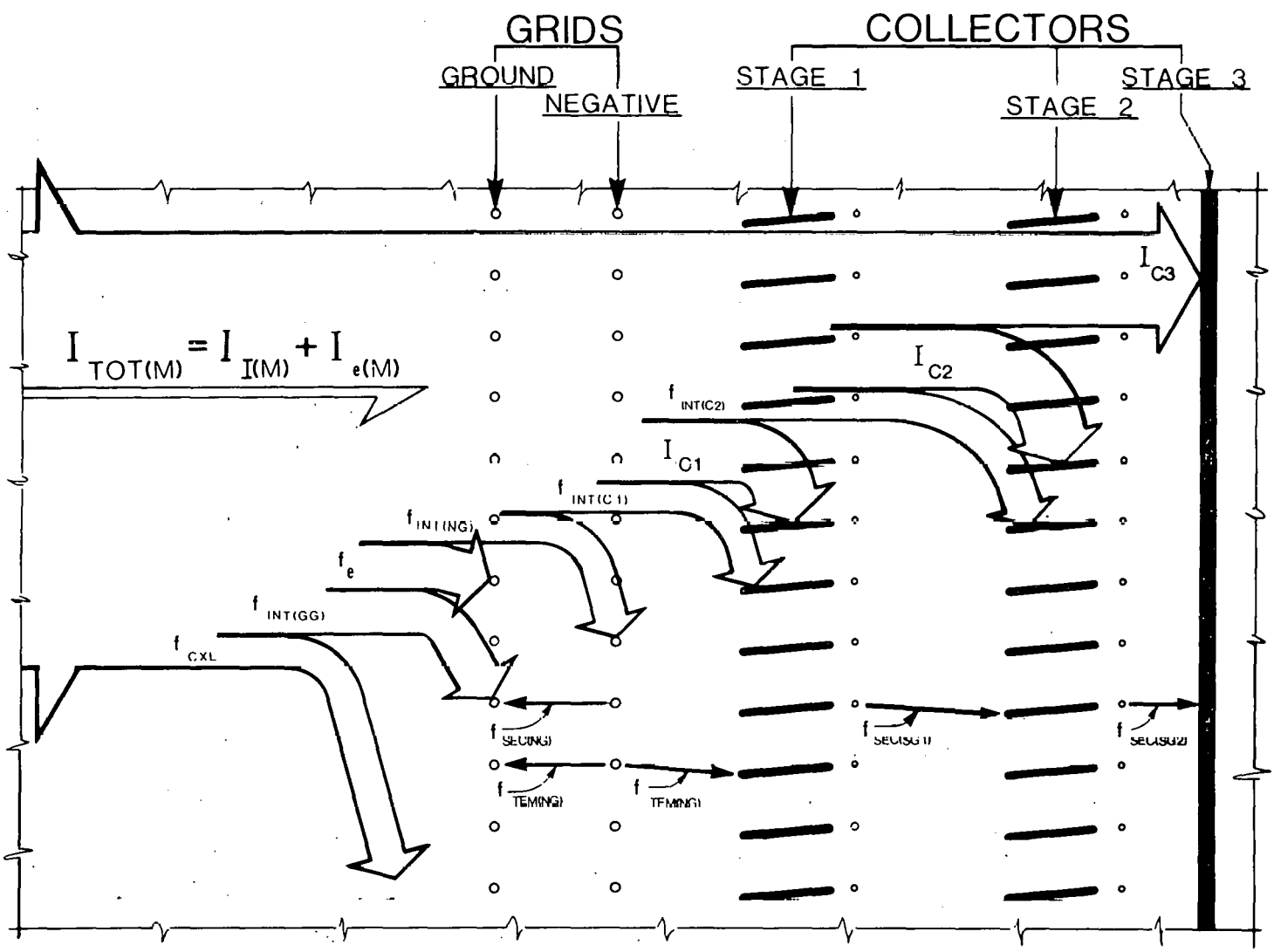

Fig. 4 Schematic diagram of the flows of the mirror leakage ions and electrons illustrating the various loss fractions.

For a desired value of f_{CXL}, this equation defines the allowable background neutral gas density, n_o in terms of the cross-section for charge exchange, $\bar{\sigma}_{CX}$, properly averaged over the ion energy distribution function and the length of the expander region, L_{EX} from the mirror exit to the collectors.

The efficiency loss due to ion interception on the grounded grid is simply

$$\Delta\eta'_{GG} = (1 - f_{CXL})\, f_{INT(GG)} \tag{4}$$

where $f_{INT(GG)}$ is the fraction of the frontal area occupied by the grids and their support structure at ground potential.

For the negative grid the three types of loss mechanisms mentioned above yield

$$\Delta\eta'_{NG} = (1 - f_{CXL})(1 - f_{INT(GG)})\, f_{INT(NG)} \left[1 + (1 + \gamma_{SEC(NG)}) \frac{|V_N|}{\bar{W}_I}\right] + \frac{I_{TEM(NG)}}{I_{I(M)}} \left[\frac{|V_N|}{\bar{W}_I} + f_{TEM(C)} \frac{V_C}{\bar{W}_I}\right] \tag{5}$$

The first term is due to the interception loss from the ion beam, while the second term represents the additional power drain on the negative grid power supply due to each ion intercepted plus γ secondary electrons emitted. The last term accounts for the thermionic emission power drains on the negative grid power supply plus the reduction of the collector power output by the fraction of the thermionic electrons, $f_{TEM(C)}$, which reach the collector plates.

The thermionic emission current can be estimated from:

$$\frac{I_{TEM(NG)}}{I_{I(M)}} = \frac{j_{(TEM)NG}\, \pi \bar{W}_I\, (1 - f_{CXL})(1 - f_{INT(GG)})\, f_{INT(NC)}}{q''_{I(INC)NG}} \tag{6}$$

where $j_{TEM(NG)}$ is given by the Richardson-Dushman equation:

$$j_{TEM(NG)} = \hat{A}_{RD} T_{NG}^2 \, e^{-\left(\frac{e\phi_W}{k\bar{T}_{NG}}\right)} \tag{7}$$

and the incident ion power flux is simply

$$q''_{I(INC)NG} = \frac{P_{I(NG)}}{A_M ER_{NG}} \times SF_{NU} \tag{8}$$

where SF_{NU} is a safety factor for nonuniform ion fluxes and where

$$P_{I(NG)} = P_{\bar{I}(M)} (1 - f_{CXL})(1 - f_{INT(GG)}) \left(1 + \frac{|V_N|}{\bar{W}_I} \right)$$

The safety factor is included to account for the additional loss due to the fact that the ion beam power flux is not uniform at the entrance to the direct converters. The effect of this flux peaking is probably most important for the thermionic emission loss from the negative grids, which tends to increase exponentially with the negative grid temperature. This effect can be included most simply by selecting a conservatively high value of the ion power flux incident on the negative grid. (In the examples given this nonuniformity safety factor was chosen to be about 1.25.) The average negative grid temperature, $\bar{T}_{NG}$, for a radiatively-cooled grid can be estimated once the enclosure temperatures and geometry are specified. For example, for a uniform enclosure temperature (i.e., for equal expander wall and collector plate temperatures, $T_{EX} = T_C$) we get simple

$$\bar{T}_{NG} \approx \left[T_{EX}^4 + \frac{q_{I(INC)NG}}{\sigma \epsilon_{NG} \pi} \right]^{\frac{1}{4}} \tag{9}$$

For an enclosure with variable temperatures, approximate equations are given in Ref. [5] and some detailed radiation transfer calculations for a specific design are given in Ref. [8].

The ion interception loss due to any support structure at ground potential is

$$\Delta\eta'_{ST} = (1 - f_{CXL})(1 - f_{INT(GG)})(1 - f_{INT(NG)}) \; f_{INT(ST)}$$

This loss can easily be modified if the structural members are at other than ground potential.

The collection efficiency loss is given by:

$$\Delta\eta'_C = \frac{I_{I(C)}\,(\bar{W}_I - V_C)}{P_{I(M)}} = \frac{I_{I(C)}}{I_{I(M)}} \left(1 - \frac{V_C}{\bar{W}_I}\right) \tag{10}$$

$$= (1 - f_{CXL})(1 - f_{INT(GG)})(1 - f_{INT(NG)})(1 - f_{INT(ST)}) \left[1 - \frac{V_C}{\bar{W}_I}\right]$$

If there were no charge exchange or interception losses, the minimum collection loss would be

$$\Delta\eta'_{C(MIN)} = \left[1 - \frac{V_C}{\bar{W}_I}\right] \tag{11}$$

and the maximum direct conversion efficiency for a SSDC would be

$$\eta_{SSDC(MAX)} = 1 - \Delta\eta'_{C(MIN)} = \frac{V_C}{\bar{W}_I} \tag{12}$$

This model assumes that the collector potential is set at the minimum ion energy, modified by the residual gyro motion due to the finite expansion ratio:

$$V_C = W_{I(MIN)} \left(1 - \frac{1}{ER_C}\right) = \left[\frac{R_{M(PL)}V_O - V_M}{R_{M(PL)} - 1} \quad \left(1 - \frac{1}{ER_C}\right)\right] \tag{13}$$

where $R_{M(PL)}$ is the mirror ratio with plasma present, and V_O and V_M are the

plasma potentials at the plasma center and at the mirror, respectively.

We will now apply these equations to the reference SSDC design.

The leakage or so-called loss-cone ion energy distribution function for the reference mirror power reactor (MPR) based on Fokker-Planck calculations is shown in Fig. 5. It can be seen that $W_{I(MIN)}$ is 100 keV, and $\overline{W}_I$ is 168 keV. The expanders of both the SSDC and the 3-stage VBDC employ the natural fringe magnetic field of the Yin Yang magnetic coil pair. The radius, R_{BFF}, height, H_{BFF}, and half-angle, $\Theta_{BFF}/2$ for this fringe B field fan is shown in Fig. 6. The reference SSDC design was chosen with an expansion ratio at the grounded grid of 25. The resulting V_C is thus about 96 kV.

The various losses have been evaluated for the specific SSDC design for the MPR of Ref. [5]. These values are listed in Table 1 and indicate that a direct conversion efficiency, η_{SSDC}, of about 48.2% could be realized for this specific design with water-cooled negative grids, and for the specific ion energy distribution function of this mirror plasma. It should be noted that a narrower ion loss-cone distribution would lead to a higher direct conversion efficiency for a SSDC.

A breakdown of the various losses and their variation with the incident ion flux on the negative grid is given in Fig. 7. The design value of the incident ion flux is related to the expansion ratio at the negative grid, ER_{NG}, by Eq. (8). As can be seen from Fig. 7, an incident ion flux of 250 W/cm^2 was used for the reference SSDC design (referred to as Case SS-I). This value was selected to limit the pumping power required for the water coolant to reasonable levels.

It can also be seen that the use of a radiatively-cooled graphite negative grid would reduce the DC efficiency by about 3.6 percentage points to a value of about 44.6% using the carbon thermionic emission data of Ref. [15].

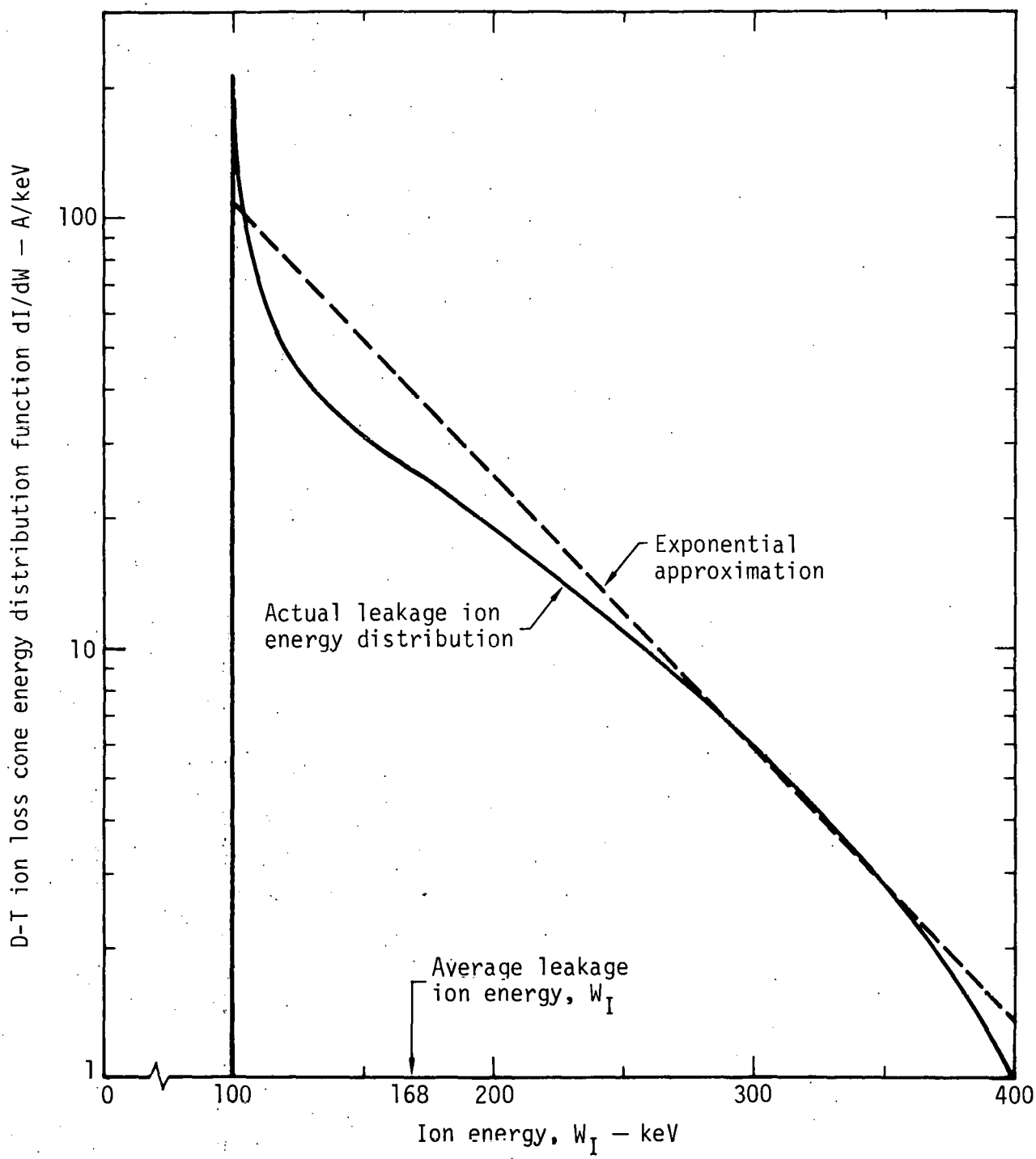

Fig. 5 Combined deuterium and tritium ion loss-cone energy distribution function for the Mirror Power Reactor design of Ref. [5].

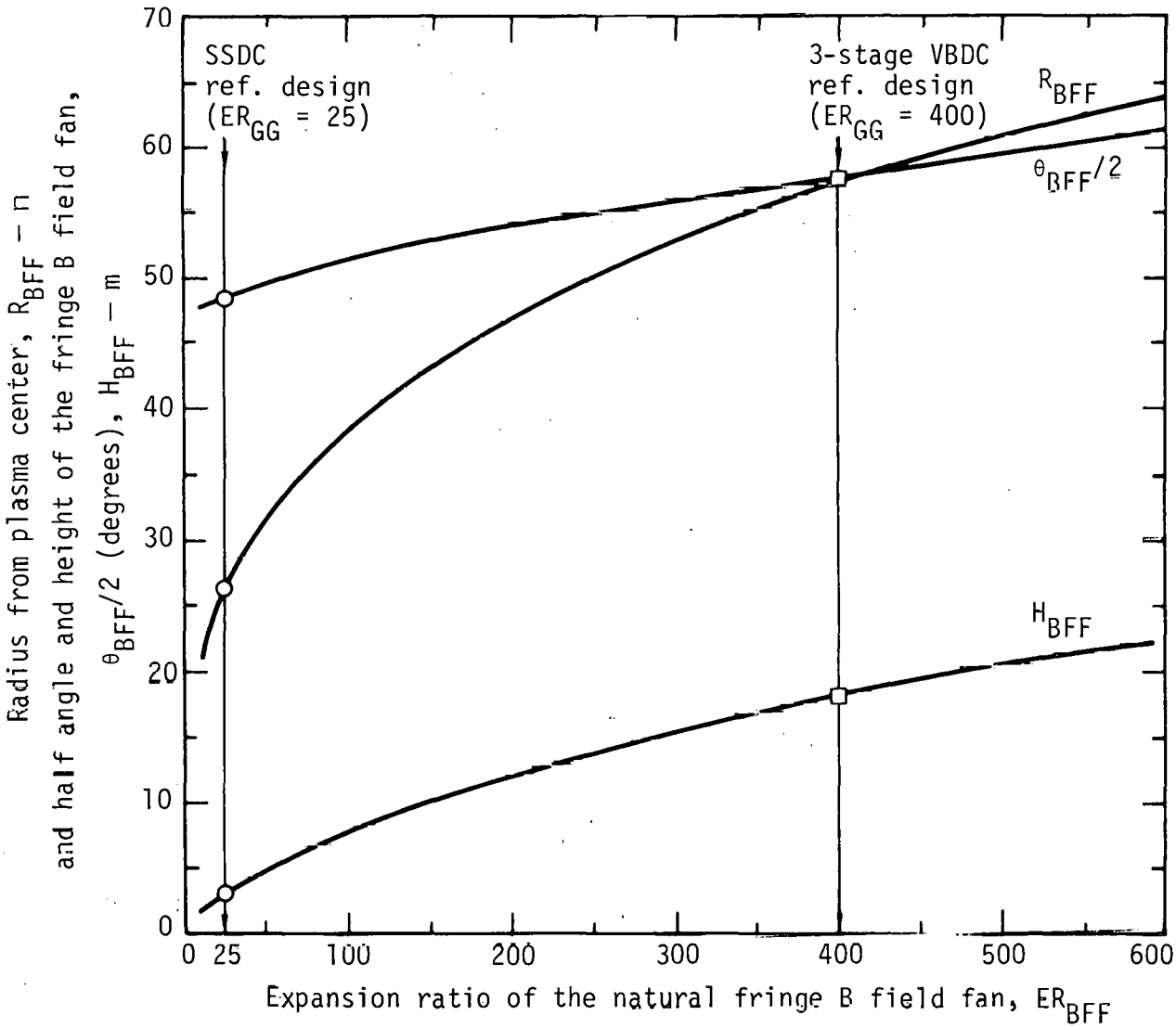

Fig. 6 Geometry of the natural fringe B field fan produced by the Yin-Yang coils of the Mirror Power Reactor of Ref. [5].

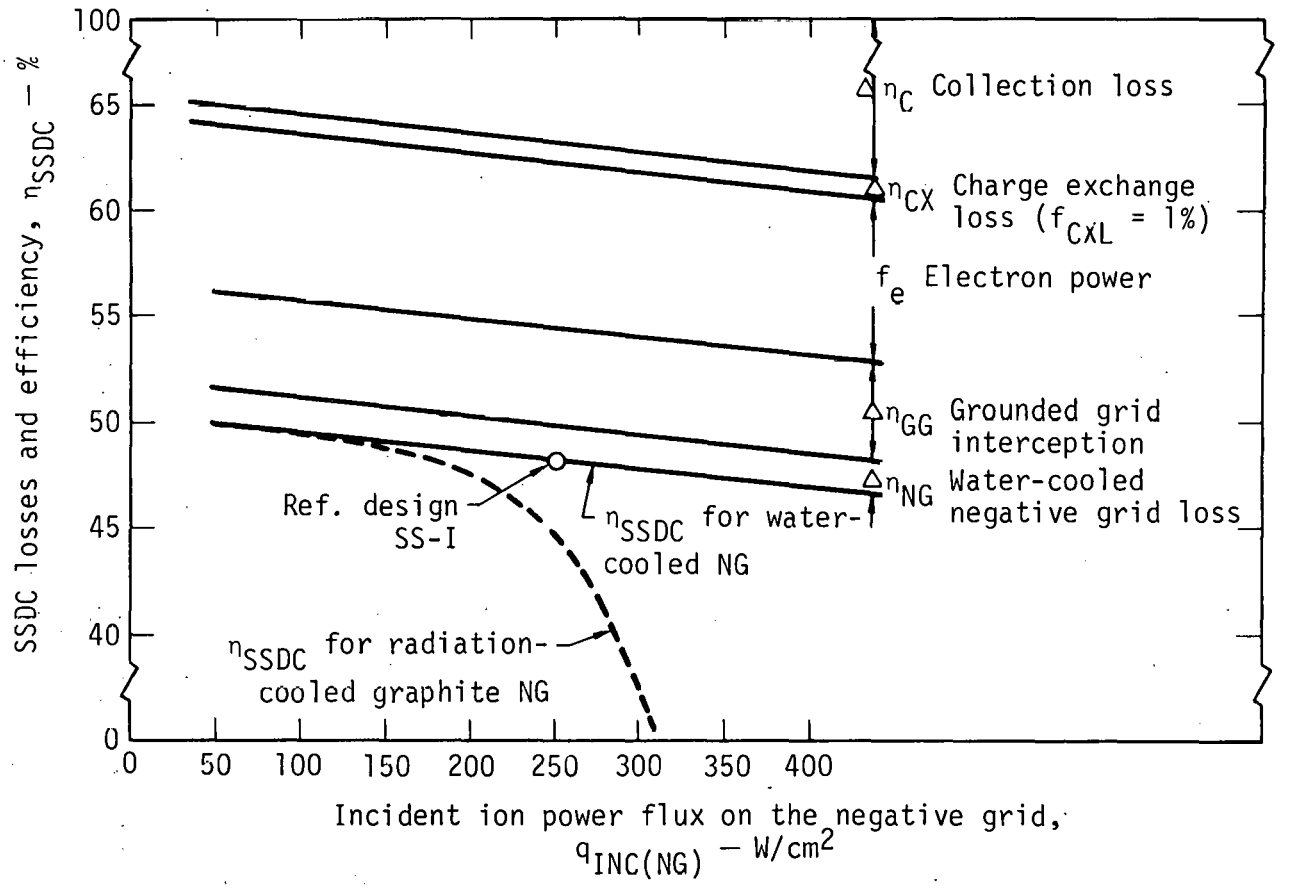

Fig. 7 Efficiency losses and final net efficiency of the reference Single Stage Direct Converter (SSDC) as a function of the incident ion power flux at the negative grid.

This may be a worthwhile price to pay for the added simplicity and reliability of a graphite mesh or woven graphite screen as compared to the water-cooled, refractory metal (Ta-10W) hollow 2 mm diameter wires in the reference design.

3. VBDC Efficiency Estimation

The basic formulation of the efficiency of a multi-stage Venetian Blind Direct Converter (VBDC) is the same as Eq. (1) for the SSDC except for the following modifications:

(a) The $\Delta\eta'_C$ must be modified to take account of the finite number of stages for multiple collector stages as well as for the initial angle of incidence of the ions relative to the plane of the collectors, α_o (see Fig. 3). This angle is required for energy sorting and reduces the normal component of the ion energy by $\cos^2\alpha_o$.

(b) The interception losses on the collection plates of all stages (except the last one) must be included and a corresponding $\Delta\eta'_{(INT)(Ci)}$ evaluated for each collector stage Ci.

(c) An additional interception loss on the collector plates must be included due to the spread in the angle of incidence, $\Delta\alpha$, due to the ion cyclotron motion in the residual B field at the collectors.

(d) The $\Delta\eta'_{ST}$ must be modified to include interception by support structure at various collector stage potentials.

(e) An additional $\Delta\eta'_{SG}$ loss term must be included to account for the secondary emission from the Suppressor Grids located behind each set of collector plates (except those in the last stage).

(f) The thermionic emission loss must be modified to account for the fraction of the thermionic electrons collected by each collector stage. As a first rough estimate it is reasonable to assume that equal percentages of the thermionic electrons are collected by each stage.

There are several additional losses in VBDC's which are usually quite small in a well-designed system. These include the non-adiabaticity of the ion

trajectories due to the field line curature in the expander, trajectory distortion in the collector region due to the residual B fields in that region; electric field distortion effects on trajectories due to the finite spacing of the grid and collector elements; and direct ion interception power loss on the suppressor grids. These losses are discussed in more detail in Refs. [5] and [10] to [14]. For simplicity, we will assume that these small losses can be neglected.

It should be noted that the reference VBDC design employs a fixed expansion ratio, $ER_{GG} = 400$ selected to insure that the trajectory distortion effect is small. At this small residual B field the average ion transit time through the collector structure is much less than a gyro period. However, if we wanted to evaluate the quantitative effects of orbit distortion, we could then develop a scaling law for the corresponding loss in DC efficiency. We might thus be able to perform some interesting trade off studies on the effect of reducing the expansion ratio of the VBDC on its efficiency and cost.

The approximate equations for the important new loss mechanisms (a) through (f) which must be included for multi-stage VBDC's are given in Appendix B and are summarized in Tables 2A and 2B.

The final efficiency equation for a three-stage VBDC can be written in terms of the losses as follows:

$$\eta_{VBDC} = (1 - f_e)\,[1 - \Delta\eta'_{CX} - \Delta\eta'_{GG} - \Delta\eta'_{NG} - \sum_{C1}^{C3}\Delta\eta'_{Ci} - \Delta\eta'_{INT(C1 - G2)} - \Delta\eta'_{INT(C1 - G3)} - \Delta\eta'_{INT(C2 - G3)} - \sum_{i=1}^{3}\Delta\eta_{SEC(SGi - Gi)} \quad (14)$$

Each of these losses has been evaluated for the reference design and the values are listed in Table 1. A feeling for the major and minor losses for this specific design and specific ion energy distribution function can be obtained

by examining this table. In particular, it can be seen that the total efficiency loss due to interception on the collector structures is only about 2.1%. The secondary emission losses only add another 0.7% to this. Consequently, it does not pay to do exceedingly detailed evaluations of these small losses for preliminary design purposes; a reasonable good approximate estimate of each of the fractional interceptions on the collector stages will usually suffice.

4. Combined DC/Bottoming Plant Efficiency

Many elements of the two types of DC's can, in principle, be designed to run at high enough temperature to make it attractive to use this energy in a thermal bottoming plant. The combined efficiency of the DC plus the bottoming plant efficiency is given by (neglecting the vacuum pumping power):

$$\eta_{COMB} = \frac{P_{E(DC)} + P_{E(BOTT)}}{P_{TOT(M)}} = \eta_{DC} + (1 - \eta_{DC})\, f_{TH(BOTT)}\, \eta_{TH(EFF)} \qquad (15)$$

where $\eta_{TH(EFF)} = (\eta_{TH} - f_{pp})$ is the thermal efficiency of the bottoming plant, η_{TH}, minus the fractional pumping power required to pump the coolant used to transfer the thermal energy from the DC to the bottoming plant.

$$f_{pp} = \frac{P_{PUMP}}{P_{TH(BOTT)}} \qquad (16)$$

For helium coolant, this is typically 1-5% in a well-designed heat removal system including the heat exchanger.

The fraction of the total thermal power which is transferred to the bottoming plant is

$$f_{TH(BOTT)} = \frac{P_{TH(BOTT)}}{P_{TH(TOT)}} = \frac{P_{TH(BOTT)}}{P_{TOT(M)}\,(1 - \eta_{DC})} \qquad (17)$$

This is evaluated for several cases of interest in Appendix C.

5. Component Cost Equations

The scaling laws for the major component costs are summarized in Table 3A, and the key constants used in this study are given in Table 3B. It should be noted at the outset that an attempt has been made to express all the costs in 1975 dollars. In addition, most of the costs, particularly for non-standard items, are essentially "first-of-a-kind" costs, since the only solid cost data available for most items was from industry bids on similar hardware for mirror fusion experiments. Finally, no allowance has been made for site preparation, engineering or contingencies in these costs. These items can increase the costs by 25% - 50%, and can be added on afterwards for the entire fusion powerplant. Each component equation is discussed briefly in Appendix D, and the design features and weight estimates for the novel Burleigh-type vacuum tank are given in Appendix E.

The basic cost-effectiveness parameter used in this study is the specific capital cost of the Direct Converter Subsystem (DCS):

$$SCC_{DCS} = \frac{C_{DCS}}{P_{E(DCS)}}$$

where $P_{E(DCS)}$ includes the electric power produced in the part of the thermal bottoming plant associated with the Direct Converter.

6. Some Cost Estimates for Direct Converters

In this section, we will examine the costs of the reference SSDC and VBDC designs for the pure fusion Mirror Power Reactor (MPR) of Ref. [5]. Then we will show how these approximate efficiency and cost equations can be used to perform a typical trade off study. In this case we will determine the charge exchange loss fraction, f_{CXL}, which results in a near minimum specific capital cost ($\$/kW_e$) of the DC Subsystem. While this is clearly a sub-optimization of only the DC Subsystem, it is still of considerable value in choosing good design parameters.

6.1 SSDC Reference Design

The reference design of the SSDC for the pure fusion MPR of Ref. [5] handles a mirror leakage power of 278 MW, 20% of the total leakage power. As mentioned previously, the reference design utilizes a water-cooled negative grid, which results in a DC efficiency of about 48.2% at an incident power flux of 250 W/cm^2. This produces a compact SSDC with an expansion ratio, $ER_{GG} = 25$, and a tank radius of only about 19.3 m (compared to about 50 m for the VBDC design with $ER_{GG} = 400$).

The total cost of the reference SSDC including the bottoming plant for 1% charge exchange loss is estimated to be about $\$51.3 \times 10^6$. This is referred to as Case SS-IA as indicated in Table 4. The total electric power produced by the combined DC and bottoming plant is about 190 MW_e, yielding an overall specific capital cost for the Direct Converter Subsystem, $SCC_{DCS} = \$270/kW_e$.

The costs of the various components of this reference SSDC design are apportioned approximately as follows:

10.4% for the vacuum tank,

18.5% for the cryopanels,

28.0% for the liquid nitrogen refrigerator,

5.1% for the liquid helium refrigerator,

1.0% for the DC modules,

13.2% for the DC power conditioning equipment,

5.0% for the thermal panels, and,

18.8% for its share of the bottoming plant.

It can be seen that the entire cryogenic vacuum pumping system is about 51.6% of the total cost in order to achieve the very low, design-point charge exchange loss fraction, f_{CXL}, of only 1%. In Section 6.3 we will examine the consequences of allowing larger charge exchange losses in an attempt to reduce this very large cost item.

It should be noted that the cryogenic method of pumping the large quantities of D_2 and T_2 gas produced when the deuterium and tritium ions become neutralized upon striking the collector plates (or some other surface) involves condensation of these gases on liquid helium cooled cryopanels. As illustrated in Fig. 8, various chevron-shaped baffles must be placed in front of the liquid helium panels to keep the heat load to the liquid helium refrigerator acceptable. If it desired to utilize the thermal energy radiated and convected toward these cryopanel assemblies in a thermal bottoming plant, high temperature thermal panels can be employed as shown in Fig. 8.

6.2 VBDC Reference Design

The reference three-stage VBDC design handles a total mirror leakage power of 1112 MW at an efficiency of 63.8% to produce about 709 MW_e of DC power for 1% charge exchange loss. The bottoming plant produces an additional 161 MW_e for a total electric power output from the DC subsystem of 870 MW_e and a combined efficiency of 78.2%. This is referred to as Case VB-IA (see Table 4).

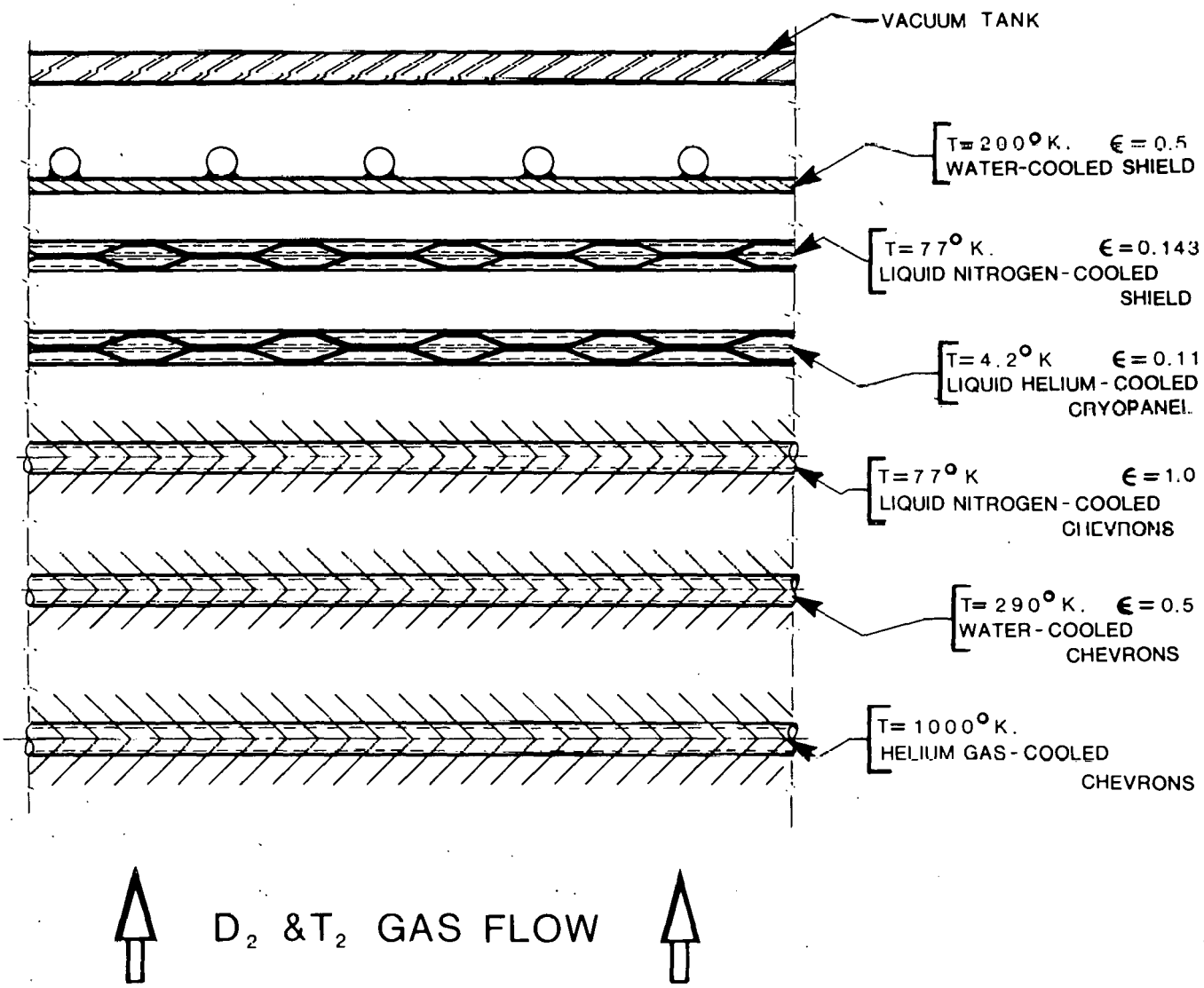

Fig. 8 Schematic diagram showing the layout of the thermal panel (TP) and cryopanel (CP) assembly with the reference temperatures and emissivities used in this study.

The total cost for this case is estimated as about $364 x 10^6, divided as follows among the components:

37.1% for the vacuum tank,

37.5% for the cryogenic vacuum system,

2.3% for the direct converter modules,

7.2% for the DC power conditioning equipment,

8.2% for the thermal panels, and

7.7% for its share of the bottoming plant.

As in the case of the SSDC, we see that the cryogenic vacuum pumping system cost is a large fraction of the total for f_{CXL} = 1%. The vacuum tank is another very large cost item for this Option A.

The specific capital cost for the entire DC Subsystem, SCC_{DCS} is about $\$418/kW_e$ for this Case VB-IA. This is considerably higher than previous estimates of about $\$133/kW_e$ of Ref. [8]. The higher cost is due in part to the choice of 1% charge exchange loss here compared to 3% in Ref. [8], and due in part to the use of updated and conservative cost estimates for many of the costly components, including the vacuum tank and the cryo-system. An additional small cost increase is due to the use of 1975 dollar estimates in this present study.

6.3 Trade Offs on Charge Exchange Losses

It is clear from the preceding cost breakdowns for both the SSDC and the VBDC that the cryogenic vacuum pumping system is exceedingly costly if we insist on only 1% charge exchange loss. As a result, a study has been made of the effect of increased charge exchange loss on efficiency and capital costs.

The DC geometry and operating voltages have been held fixed in this trade off study. Only f_{CXL} and the associated cryopanel area and refrigerator capacity change significantly. There are, however, some changes in the costs of the bottoming plant and the DC power conditioning equipment as the power

handled by each component changes with f_{CXL}. The thermal power associated with the charge exchange neutrals is assumed to be lost from the ion beam before reaching the DC, but it is assumed to be absorbed by the thermal panels or collector plates where the neutrals impinge and transferred to the thermal bottoming plant by high-pressure, high-temperature helium coolant (typically at 60 atm. and about 900 K).

The variations of the DC efficiency and the combined DC plus bottoming plant efficiency for both direct convertor designs are shown in Fig. 9. It can be seen that all the efficiencies decrease almost linearly as f_{CXL} increases. However, as expected, the combined DC Subsystem efficiency decreases more slowly than the efficiency of the DC alone, because of the recovery of part of the charge exchange thermal power in the bottoming plant.

The variation of the total capital cost of the DC Subsystem is shown in Fig. 10. The most prominent feature of all these curves is the rapid decrease in cost as f_{CXL} is increased from 1% to about 10%. For the VBDC design (Option A), the cost decreases almost 31% from Case VB-IA to Case VB-IIA. This reduction in cost is also graphically illustrated on Fig. 11. For the 33DC design, the corresponding decrease is about 46%. These decreases are due almost entirely to reductions in the cryopanel area (and hence the entire cryo-system cost) required to achieve the background neutral gas density for 10% charge exchange loss instead of 1% loss.

The variation of the total DC Subsystem specific capital costs, SCC_{DCS}, with f_{CXL} is shown in Fig. 12. This is the best measure of cost-effectiveness for the DC Subsystem by itself short of going to an estimate of the specific generating costs for electricity in mills/kW_e-hr. Figure 12 clearly shows that operation at a charge exchange loss of about 10% is much more cost-effective

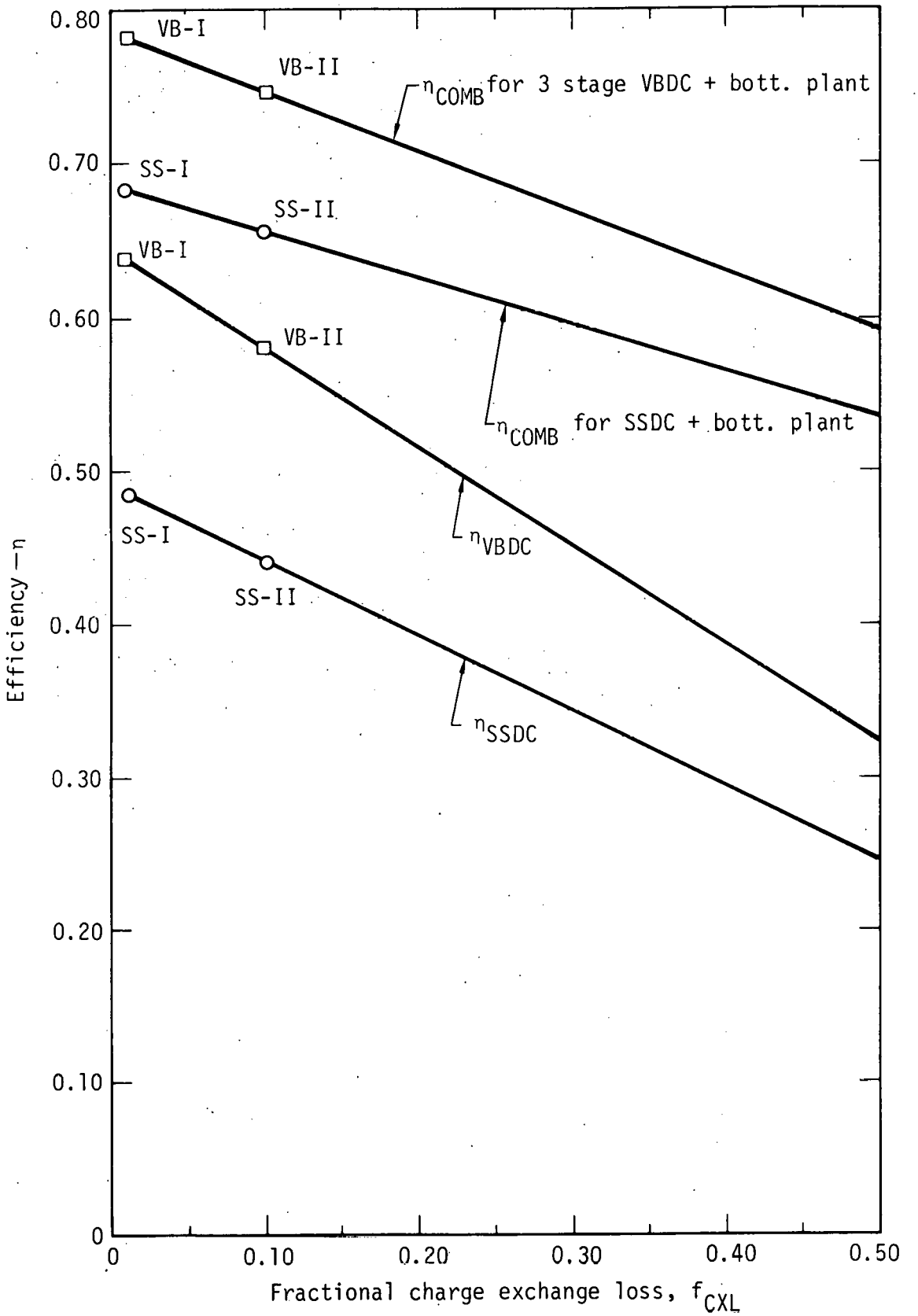

Fig. 9 Direct converter efficiencies and combined direct converter plus thermal bottoming plant efficiencies as a function of the charge exchange loss fraction in the expander region.

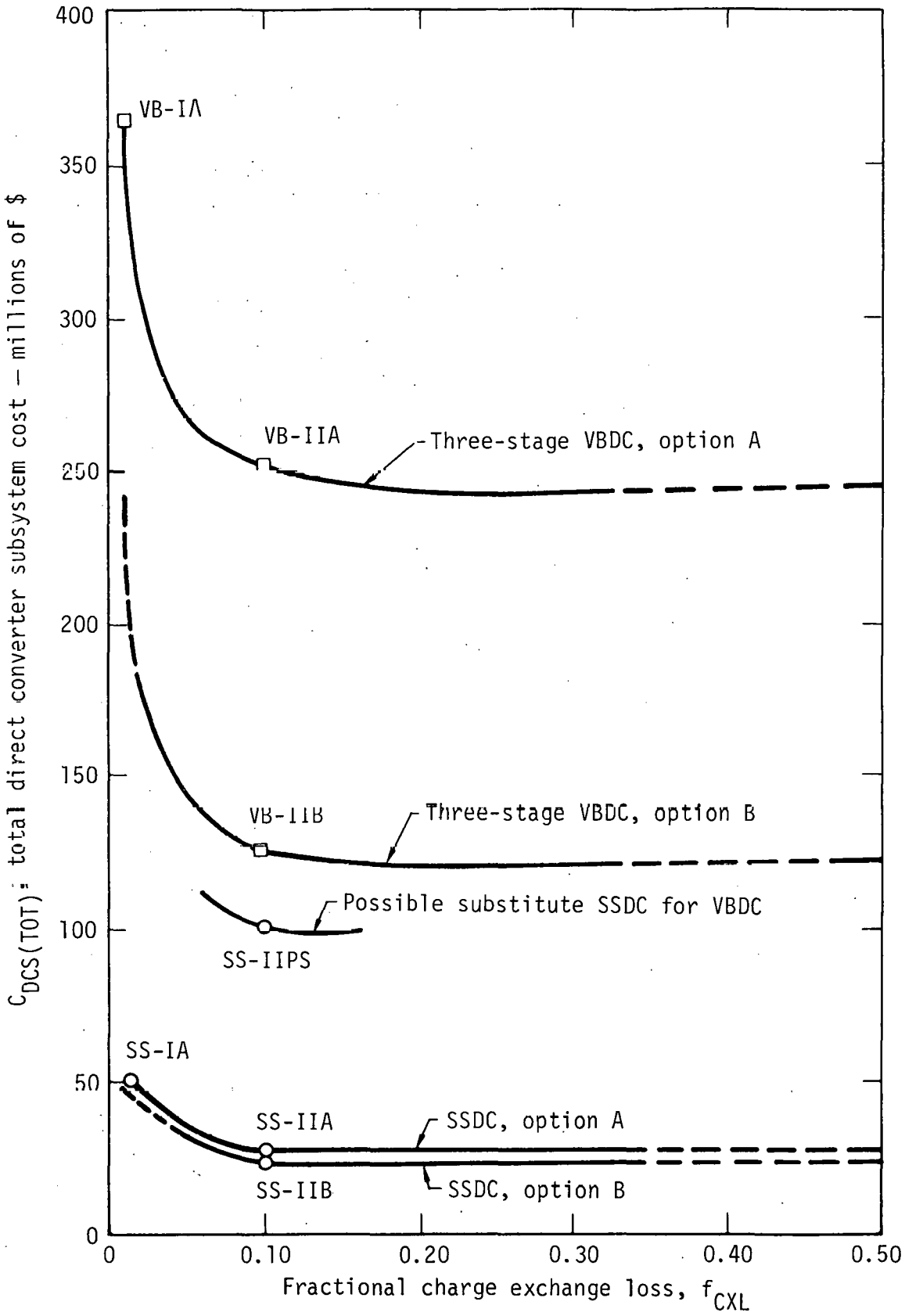

Fig. 10 Total direct converter subsystem costs for several important options as a function of the charge exchange loss fraction.

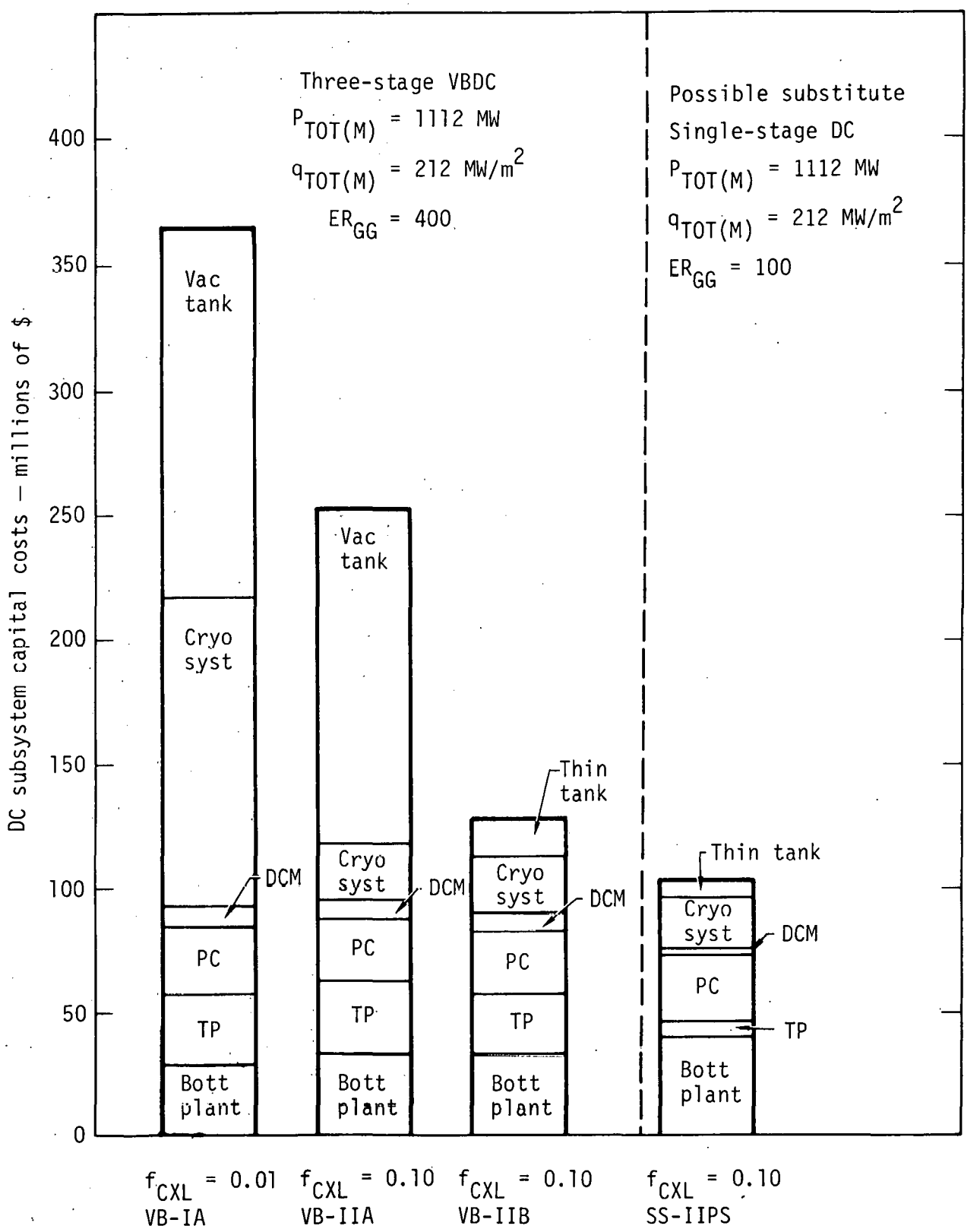

Fig. 11 Cost breakdown for the three-stage Venetian Blind Direct Converter (VBDC) for three cases of interest, and comparison with a possible substitute SSDC.

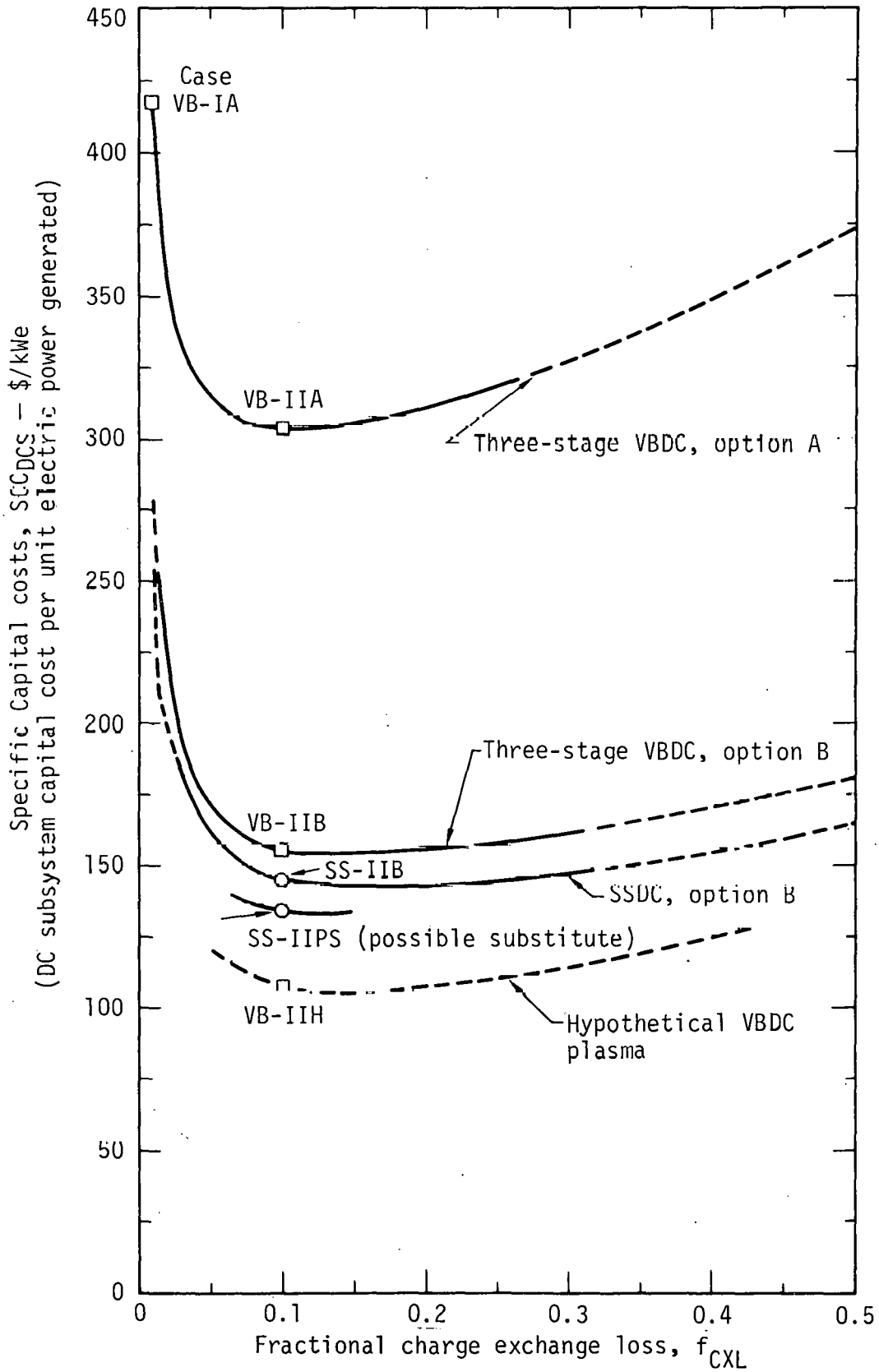

Fig. 12 Specific capital costs for several important direct converter subsystem options as a function of the charge exchange loss fraction.

for all the cases studied than the nominal value of 1% chosen somewhat arbitrarily for the reference designs.

From the top curve on Fig. 12, we see that the specific capital cost of the VBDC design decreases almost 27% in going from Case VB-IA (f_{CXL} = 1%) to Case VB-IIA (f_{CXL} = 10%). The cost breakdowns are given by the first two bar graphs on Fig. 11. The corresponding decrease for the SSDC design is about 43%. (Note that the SSDC curve for Option A is not shown on Fig. 12 because it is so close to the VBDC curve for Option B, to be discussed in a moment).

We can thus conclude that within the framework and limitations of this suboptimization study, it is obviously better to allow about 10% charge exchange loss. However, it should be noted that there are limitations on the maximum allowable background neutral gas density, n_o, and hence the maximum f_{CXL}, which can be tolerated. While this limit on n_o in the expander region is still not well-defined numerically, it is well-known that too high an n_o can create several problems for the reactor plasma and/or the first wall. For example, if n_o is too large the backflow into the reactor of neutrals and/or cold electrons produced by ionizing collisions could cause significant charge exchange reactions just inside the mirror point. The high energy neutrals could then cause serious sputtering of the walls and also flood the reactor plasma with cold secondary electrons.

As a final caution, we must be careful not to try to compare costs of these particular VBDC's and SSDC's. This is due to the fact that the VBDC is designed to handle a mirror leakage power flux of about 212 MW/m^2 (from the weaker mirror), while the SSDC is designed to handle a mirror leakage power flux of one quarter this value, namely 53 MW/m^2. In the next section we will discuss a possible substitute SSDC for the VBDC which is specifically designed to handle the higher mirror leakage power flux, so that meaningful comparisons

can be made.

6.4 Additional Possible Cost Reductions

As can be seen from Fig. 11, Case VB-IIA, the vacuum tank is the major cost item left once the cryo-system cost has been reduced by going to 10% charge exchange loss. As mentioned previously, Option A is for these cases where a separate Burleigh-type vacuum tank is placed around each DC (see Table 4).

An alternative Option B would be to place the entire reactor plus direct converters inside a large vacuum building which also serves as the tritium containment building. This eliminates the need for vacuum-tight welds on much of the reactor blanket structure as well as the need for a separate vacuum tank for each DC. The concept also has many other potential advantages which are described in Ref. [16].

For this Option B, only a thin-walled, fan-shaped membrane tank sufficiently strong to support the loads of its own weight plus the weight of the various cryopanels, thermal panels and direct converter modules would be required. It is estimated [17] that such a thin tank would require an average wall thickness on the order of 1 cm, which is the figure used for the weight estimates in this paper.

For the reference VBDC design, this Option B results in a thin tank weight of about 0.96×10^6 kg and a cost of only about $\$12.7 \times 10^6$. The cost of the VBDC Subsystem is greatly reduced for this Option B compared to Option A as can be seen in Figs. 10 and 11. (A much smaller cost reduction results for the SSDC as shown on Fig. 10.) However, it should be noted that no penalty for the additional cost of the large vacuum containment building has been included in this study. A complete reactor systems analysis is required to see if the overall result of using a large vacuum building is a cost reduction.

The specific capital cost of the VBDC Subsystem is also dramatically

reduced from about $306/kW_e for Case VB-IIA to only about $156/kW_e for Case VB-IIB (Fig. 12). This is about the best SCC value found in this study for a VBDC which can handle a mirror leakage power of 1112 MW at a mirror power flux of 212 MW/m^2.

It is of interest to ask what the efficiency and cost of a Possible Substitute SSDC would be to handle this same 1112 MW at the same mirror power flux level. In order to limit the incident ion flux on the negative grid to about 250 W/cm^2, an expansion ratio of about 100 is required (i.e., about 4 times the expansion ratio for the reference SSDC design which handles only 278 MW, one quarter of the above power).

The efficiency of this Possible Substitute SSDC for Case SS-IIPS (10% charge exchange loss) is about 47% compared to about 58% for the VBDC with the same charge exchange loss. However, as shown on Figs. 10 and 11, the cost of this SSDC is only about $\$100 \times 10^6$. This yields a specific capital cost of only about $\$135/kW_e$ compared to the best VBDC (Case VB-IIB) of $\$156/kW_e$. We should also note that the size and cost of the vacuum building necessary to cover the reactor with this substitute SSDC (where $R_T \approx 31$ m) would be less than the one to house the reactor with the three-stage VBDC attached (where $R_T \approx 50$ m).

Many more interesting comparisons could be made using the efficiency and cost scaling laws presented. However, the examples given in this section should suffice to illustrate their utility. Some additional examples are given in Appendix F.

7. Summary and Conclusions

The following general summary comments can be made:

(a) Simple approximate equations to model the efficiency and costs of specific types of electrostatic direct converters have been presented.

(b) While these equations are based on the specific reference designs for the SSDC (Single Stage Direct Converter) and the three-stage VBDC (Venetian Blind Direct Converter) for the Mirror Power Reactor study of Ref. [5], it should be relatively easy to modify the equations for many variations of these design concepts.

(c) These equations are primarily intended for use in large overall fusion reactor systems codes for evaluating fusion powerplant performance and costs and for selecting the "best" reference design parameters for detailed conceptual design studies.

For the three-stage VBDC reference design for the Mirror Power Reactor, which handles a mirror leakage power of 1112 MW (at a mirror leakage power flux of 212 MW/m^2), the following specific conclusions can be drawn based on the trade off studies and the suboptimization of only the DCS (Direct Converter Subsystem consisting of the direct converter and its share of the thermal bottoming plant):

(a) The dominant cost items for this VBDC design with its required expansion ratio of 400 and with only 1% charge exchange loss (Reference Case VB-IA) are the cryogenic vacuum pumping system (37.5%) and the vacuum tank (37.1%). The specific capital cost for this case is estimated to be about $\$418/kW_e$.

(b) It appears to be cost-effective to allow about 10% charge exchange loss. For this Case VB-IIA, the specific capital cost is reduced to about $\$306/kW_e$, a reduction of about 27%.

(c) If the tritium containment building which houses the entire reactor

"nuclear island" plus the direct converters is designed as a vacuum building, the individual vacuum tanks for the direct converters can be dispensed with. Assuming only a thin, fan-shaped membrane tank strong enough to support the DC modules, cryopanels and thermal panels, the specific capital cost can be reduced to only \$156/kW_e (Case VB-IIB with 10% charge exchange loss). However, it should be noted that none of the additional cost of the vacuum building has been included in this figure.

(d) We can compare the above cost figure in paragraph (c) to that for a Possible Substitute SSDC which can handle the same mirror leakage power flux of 212 MW/m^2. For the required expansion ratio of only 100 (compared to 400 for the VBDC), the specific capital cost is about \$135/kW_e (Case SS-IIPS with 10% charge exchange loss). The lower cost of the thermal panels required to cover the smaller expander wall area more than compensates for the lower DC efficiency of the Substitute SSDC (about 47% for Case SS-IIPS) compared to the three-stage VBDC (about 58% for Case VB-IIB).

For the SSDC reference design for the Mirror Power Reactor, which handles a mirror leakage power of 278 MW (about 53 MW/m^2 of mirror leakage power flux, only one quarter of the value for the VBDC), the following specific conclusions can be drawn:

(a) As for the VBDC, an increase in the allowable charge exchange loss from 1% to 10% and the use of a thin membrane tank reduce the specific capital costs of the SSDC from about \$270/kW_e (for Case SS-IA) to about \$146/kW_e (for Case SS-IIB).

(b) The use of thermal panels on the expander walls of this SSDC to recover the thermal power from the charge exchange neutrals is probably not cost-effective. Even at the rather high value of 10% charge exchange loss, the

total specific capital costs with thermal panels is about \$146/kW_e (Case SS-IIB) which is higher than the estimated value of \$140/kW_e without them.

(c) The use of a radiation-cooled graphite negative grid in place of the water-cooled negative grid of the reference SSDC design would reduce the DC efficiency by about 3.6% (and the combined DC plus bottoming plant efficiency by about 1.5%). This penalty seems acceptable since a simpler and more reliable negative grid structure of graphite mesh or a woven graphite screen can be used.

(d) We must not make the mistake of trying to directly compare costs of this reference SSDC design which handles only 53 MW/m^2 of mirror leakage power flux with the VBDC design which handles 212 MW/m^2 even though the results are plotted on the same figures (Figs. 10 and 12) for convenience.

(e) An SSDC is a compact and efficient means for slowing down the plasma leakage from an open fusion reactor. The alternative of going to a simple "plasma dump" or plasma thermal converter may prove to be no more compact and perhaps less cost-effective than an SSDC. Comparison studies of these two alternatives are certainly warranted.

References

[1] W. L. Barr, et al, Apparatus for Testing Direct Energy Conversion of Plasma Energy to Electricity, UCRL-75174, Lawrence Livermore Lab., Nov. 6, 1973.

[2] R. W. Moir, W. L. Barr and G. A. Carlson, Direct Conversion of Plasma Energy to Electricity for Mirror Fusion Reactors, UCRL-76051, Lawrence Livermore Lab., Sept. 24, 1974.

[3] W. L. Barr and R. W. Moir, A Review of Direct Energy Conversion for Fusion Reactors, UCRL-78204, Lawrence Livermore Lab., Sept. 20, 1976.

[4] D. J. Bender and G. A. Carlson, System Model for Analysis of the Mirror Fusion-Fission Reactor, UCRL-52293, in preparation, Lawrence Livermore Laboratory.

[5] R. Moir, et al, Reference Mirror Power Reactor Conceptual Design Study, in preparation, Lawrence Livermore Laboratory.

[6] R. W. Werner, Mirror Machines and Direct Conversion, UCRL-72487, Lawrence Livermore Lab., May 26, 1970.

[7] B. H. Smith, R. J. Burleigh, W. L. Dexter and L. L. Reginato, An Engineering Study of the Electrical Design of a 1000 Megawatt Direct Converter for Mirror Reactors, UCRL-74047, Lawrence Livermore Lab., Nov. 27, 1972.

[8] W. L. Barr, R. J. Burleigh, W. L. Dexter, R. W. Moir and R. R. Smith, A Preliminary Engineering Design of a "Venetian Blind" Direct Energy Converter for Fusion Reactors, IEEE Trans. on Plasma Science, Vol. PS-2, June 1974, pp. 71-92.

[9] R. W. Moir, et al, Progress on the Conceptual Design of a Mirror Hybrid Fusion-Fission Reactor, UCRL-51797, Lawrence Livermore Lab., June 25, 1975.

[10] R. W. Moir and W. L. Barr, "Venetian Blind" Direct Energy Converter for Fusion Reactors, Nuclear Fusion, Vol. 13, 1973, pp. 35-45.

[11] W. L. Barr, Some Considerations in the Design of a Venetian Blind Direct Converter, UCID-16985, Lawrence Livermore Lab., Dec. 15, 1975.

[12] R. W. Moir and J. D. Lee, Criteria for Design of an Adiabatic Expander for a Direct Energy Converter, TID-4500, UC-20, Lawrence Livermore Lab., Feb. 15, 1973.

[13] R. W. Moir, W. L. Barr and G. H. Miley, Surface Requirements for Electrostatic Direct Energy Converters, J. Nucl. Mats., 53, 1974, pp. 86-96.

[14] A. S. Blum, Advanced-Fueled Fusion Reactors Suitable for Direct Energy Conversion, Lawrence Livermore Lab:

a) Expander Structure, UCRL-79061, Jan. 20, 1977.

b) Single-Stage Converter Performance Analysis, UCRL-79062, Jan. 20, 1977.

c) An Extension of the Single-Stage Direct Converter Analysis to the Venetian Blind Direct Converter, in preparation.

[15] S. C. Jain and K. S. Krishnan, The Thermionic Constants of Metals and Semiconductors, Pt. I-Graphite, Proc. Royal Society A-213, p. 143, June 24, 1952.

[16] R. W. Werner, ORNL Fusion Power Demonstration Study: Arguments for a Vacuum Building, ORNL-TM-5664, Dec. 1976.

[17] J. Doggett, personal communication, Lawrence Livermore Lab., April, 1977.

[18] F. H. Coensgen, MX Major Project Proposal, LLL-Prop-142, Lawrence Livermore Lab., March 15, 1976.

[19] T. R. Strobridge, Cryogenic Refrigerators - An Updated Survey, Cryogenics Div., NBS, June, 1974.

[20] An Evaluation of the Technical and Economic Feasibility of Mirror Fusion Devices, Bechtel Final Rept., UCRL-13695, Aug., 1976.

Acknowledgements

The author wishes to acknowledge the many useful discussions with several Lawrence Livermore Laboratory researchers including W. L. Barr, D. Bender, A. Blake, A. S. Blum, G. A. Carlson, J. Doggett, J. D. Lee, R. Moir, W. Neef and R. Werner.

This work was supported by U. S. Energy Research and Development Administration Contract W-7405-ENG-48 (LLL).

TABLE 1

Direct Converter Efficiencies and Losses for the Reference Designs of the Mirror Power Reactor Study (Ref. [5])

	Nominal Ref. Design Parameters Used	Reference SSDC	Reference 3-Stage VBDC
f_e	----------	.0777	.0777
$\Delta\eta_{CX}$	$f_{CXL} = .01$	.0092	.0092
$\Delta\eta_{GG}$	$f_{INT(GG)} = .05$	.0456	.0456
$\Delta\eta_{NG}$	Water-cooled for SSDC Rad-cooled for VBDC $f_{INT(NG)} = .01$ for SSDC $f_{INT(NG)} = .02$ for VBDC	.0177	.0384
$\Delta\eta_C$	$ER_C \simeq 25$ for SSDC $ER_C \approx 400$ for VBDC $\alpha_o = 8.0^o$ for VBDC	.3680	.1620
$\Delta\eta_{INT(C1)}$	$f_{INT(C1-G2)} \simeq .087$ for VBDC	-	.0074
	$f_{INT(C1-G3)} \simeq .086$ for VBDC	-	.0093
$\Delta\eta_{INT(C2)}$	$f_{INT(C2-G3)} \simeq .080$ for VBDC	-	.0047
$\Delta\eta_{SEC(SG1-G1)}$	$\gamma_{SEC} \approx 2.5$	-	.0041
$\Delta\eta_{SEC(SG2-G2)}$	$f_{INT(SGi-Gi)} = .01$	-	.0033
$\Sigma\Delta\eta_{losses}$		.518	.362
η_{DC}		.482	.638

TABLE 2A - Summary of Simplified Efficiency Loss Equations for Multistage VBDC's

$$\eta_{VBDC} = 1 - f_e - \Delta\eta_{CX} - \Delta\eta_{GG} - \Delta\eta_{NG} - \Sigma\Delta\eta_{Ci} - \Sigma\Delta\eta_{INT(Ci-Gj)} - \Sigma\Delta\eta_{SGi}$$

Loss	Direct Conversion Efficiency Loss Equation
Electron power	$\Delta\eta_e \equiv f_e$
Charge exchange	$\Delta\eta_{CX} = (1-f_e)\, f_{CXL}$
Grounded Grid Interception	$\Delta\eta_{GG} = (1-f_e)\,(1-f_{CXL})\, f_{INT(GG)}$
Negative Grid Total Losses	$\Delta\eta_{NG} = (1-f_e)(1-f_{CXL})\left(1-f_{INT(GG)}\right) f_{INT(NG)} \left[1+\left(1+\gamma_{SEC(NG)}\right)\frac{\lvert V_N\rvert}{\bar{W}_I}\right] + (1-f_e)\frac{I_{TEM(NG)}}{I_{I(M)}}\left[\frac{\lvert V_N\rvert}{\bar{W}_I} + \left(\sum f_{TEM(Ci)}\,\frac{V_{Ci}}{\bar{W}_I}\right)\right]$
Finite Number of Collector Stages	$\Delta\eta_{Ci} = (1-f_e)(1-f_{CXL})\left(1-f_{INT(GG)}\right)\left(1-f_{INT(NG)}\right)\left[\frac{\bar{W}_{Gi}-V_{Ci}}{\bar{W}_I}\right]\frac{I_{Gi(ID)}}{I_{I(M)}}\prod_{k=1}^{i-1}\left(1-f_{INT(Ck-Gi)}\right)$
Total Interception on Collectors	$\Delta\eta_{INT(Ci-Gj)} = (1-f_e)(1-f_{CXL})\left(1-f_{INT(GG)}\right)\left(1-f_{INT(NG)}\right)\left[\prod_{k=1}^{i-1}\left(1-f_{INT(Ck-Gj)}\right)\right] f_{INT(Ci-Gj)}\left[\frac{V_{Cj}-V_{Ci}}{\bar{W}_I}\right] \times \frac{I_{Gj(ID)}}{I_{I(M)}}$
Secondary Emission from Suppr. Grids	$\Delta\eta_{SEC(SGi-Gi)} = (1-f_e)(1-f_{CXL})\left(1-f_{INT(GG)}\right)\left(1-f_{INT(NG)}\right)\left[\prod_{k=1}^{i} 1-f_{INT(Ck-Gi)}\right] f_{INT(SGi-Gi)}\,\gamma_{SEC(SGi-Gi)} \times \left[\frac{V_{C(i+1)}-V_{SGi}}{\bar{W}_I}\right] \times \frac{I_{Gi(ID)}}{I_{I(M)}}$

TABLE 2B - Summary of Loss Fraction Equations for Multi-Stage VBDC's

Loss	Approximate Equations for Loss Fraction
Electron power	$f_e = P_{e(M)} / P_{TOT(M)}$
Charge exchange	$f_{CXL} = 1 - \exp\left[-\eta_o \bar{\sigma}_{CX} L_{EX}\right]$; $\bar{\sigma}_{CX} \approx 1.0 \times 10^{-19} \exp\left[-\bar{W}_I / 63.3\right]$ (m^2)
Grounded Grid Interception	$f_{INT(GG)} = A_{GG(Frontal)} / (A_M \times ER_{GG})$
Negative Grid Interception	$f_{INT(NG)} = A_{NG(Frontal)} / (A_M \times ER_{NG})$
Negative Grid Thermionic Emission	$\frac{I_{TEM(NG)}}{I_{I(M)}} \approx \frac{1}{SF_{NU}} \left[\hat{A}_{RD} T_{NG}^2 \exp\left(-e\phi_{W/kT}\right)_{NG} \left(A_M ER_{NG} \pi f_{INT(NG)}\right) \left(1+\frac{\lvert V_N \rvert}{\bar{W}_I}\right)^{-1} \frac{1}{I_{I(M)}}\right]$
Collector Ci Interception of Ion Group Gj	$f_{INT(Ci-Gj)} \approx \left\{\frac{L_i}{H_i}\left\lvert \frac{\alpha_o}{\sqrt{1-V_{Ci}/(\bar{W}_{Gj}\cos^2\alpha_o)}} - \alpha_i \right\rvert + \frac{\delta_i}{H_i}\right\}$ $\div \left[\frac{K_{SAI}}{ER_{GG}} \eta_{C(ID)} + \Delta f_{INT(ST)}\right]$ (Ci-Gj)
Suppressor Grid Interception of Ion Group Gi	$f_{INT(SGi-Gi)} \approx \left[A_{SGi(Frontal)} / \left(A_M ER_{SGi}\right)\right] \cos\alpha_o$

TABLE 3A - Summary of Simplified Cost Equations for the DC Subsystem

Component	Approximate Cost Equations (SI Units Except for Powers in kW)
Burleigh-Type Vacuum Tank	$C_{BT} = \tilde{C}_{BT}\, W_{BT}$; $W_{BT} \approx K_{BT}\, R_T^3 \left[\left(\frac{H_T}{R_T}\right)^{1.4} \left(\frac{\Theta_T}{360} + 0.32\right) + 0.21\, \frac{\Theta_T}{360}\right]$; $\left(\Theta_T < 360^o\right)$
Thin-walled Tank	$C_{TT} = \tilde{C}_{TT}\, W_{TT} \approx \tilde{C}_{TT}\, A_T\, \bar{\delta}_{TT}$
Cryo-panels	$C_{CP} = \tilde{C}_{CP}\, A_{CP}$; Reqd. $A_{CP} = k_{CP} \frac{I_{DT(M)}\, L_{EX}\, \bar{\sigma}_{CX}}{f_{CXL}\quad K_{B(EFF)}} \sqrt{\frac{293}{\bar{T}_{DT}}} \sqrt{\frac{\bar{M}}{29}} \equiv \frac{K_{CP}}{f_{CXL}}$
Cryo-refrigerators	$C_{CR} = \tilde{C}_{CR} \left\{k_{CR} \left(\frac{T_a}{T_R} - 1\right) \left[\dot{Q}_{TOT}(kW)\right]^{1-m}\right\}^{0.7} = K_{CR}\, A_{CP}^{0.7(1-m)}$
Direct Converter Modules	$C_{DCM} = \tilde{C}_{DCM}\, A_M\, ER_{GG}$
DC Power Conditioning	$C_{PC} = \tilde{C}_{PC}\, P_{e(DC)} = \tilde{C}_{PC}\, \eta_{DC}\, P_{TOT(M)}$
Thermal Panels	$C_{TP} = \tilde{C}_{TP}\, A_{EX}$
Bottoming Plant	$C_{BOTT} = \tilde{C}_{BOTT}\, P_{e(BOTT)} = \tilde{C}_{BOTT} \left(1-\eta_{DC}\right) f_{TH(BOTT)}\, \eta_{TH(EFF)}\, P_{TOT(M)}$

TABLE 3B - Summary of Numerical Values Used in the Cost Tradeoff Examples

Component	Specific Costs*	Other Constants and Auxiliary Relations Required
Burleigh-type Vacuum Tank	$\tilde{C}_{BT}$ = \$13.2/kg for stainless steel	$K_{3T} = 196.4$; $A_T = A_{membranes} + A_{sides} + A_{end} \approx 2\pi R_T^2\left(\frac{\Theta_T}{360}\right) + H_T R_T + 2\pi H_T R_T\left(\frac{\Theta_T}{360}\right)$
Thin-walled Tank	$\tilde{C}_{TT}$ = \$13.2/kg for stainless steel	A_T = same as above
Cryopanels	$\tilde{C}_{CP}$ = \$6300/m^2	$k_{CP} = 2.69 \times 10^{16}$; $L_{EX} \approx R_{GG} - R_M$; $K_{B(EFF)} \approx 0.10$; $f_s \approx 1.0$ $\bar{M} \approx 4.66$ for D-T molecules, $\bar{T} \approx 1000$ K
Cryo-Refrigerators	$\tilde{C}_{CR}$ = \$40,000	$k_{CR} = 7.30$; $m = 0.136$ $T_a \approx 300$ K ; $T_{R(LHe)} = 4.2$ K ; $T_{R(LN_2)} = 77$ K
Direct Convertor Modules	$\tilde{C}_{DCM}$ = \$4000/m^2 of frontal area	$A_M = 5.25\ m^2$ for the MPR design
DC Power Conditioning	$\tilde{C}_{PC}$ = \$46/kW_e	
Thermal Panels	$\tilde{C}_{TP}$ = \$3300/m^2	$A_{EX} \approx A_{membranes} + A_{sides} \approx 2\pi R_T^2\left(\frac{\Theta_T}{360}\right) + H_T R_T$
Bottoming Plant	$\tilde{C}_{BOTT}$ = \$175/kW_e	Steam power plant $\eta_{TH(EFF)} \approx 40\%$

*Estimated in 1975 dollars; First-of-a-kind costs

TABLE 4

Summary of Design Cases Referred to in the Text and Figures

Option	Tank Type	Case	3-Stage VBDC			SSDC(**)		
			f_{CXL}	ER_{GG}	$P_{TOT(M)}^{(*)}$ (MW)	f_{CXL}	ER_{GG}	$P_{TOT(M)}^{(*)}$ (MW)
A	Vacuum Tank (Burleigh Tank design, $\theta_{BT} = 180^{o}$)	IA	.01	400	1112	.01	25	278
		IIA	.10	400	1112	.10	25	
B	Thin Fan Tank ($\theta_{TT} \approx \theta$ of B field fan)	IIB	.10	400	1112	.10	25	278
H	Same as Option B (Hypothetical VBDC)	IIH	.10	400	4448	---	---	---
PS	Same as Option B (Possible Substitute SSDC for VBDC)	IIPS	---	---		.10	100	1112

(*) Mirror exit area was 5.25 m^2 for all cases.
(**) SSDC cases were all for a water-cooled negative grid.

Appendix A - Relation of Key DC Subsystem Parameters to Overall Fusion Powerplant System Parameters

In fusion reactor systems studies, it is desired to calculate the overall power plant performance and costs using a reasonably complete, but simplified model of each component or subsystem. Then optimization studies are performed in an attempt to define the power plant with the lowest generating costs of electricity for pure fusion concepts (or more complex cost-effectiveness parameters in hybrid fusion-fission reactors) consistent with the physics and engineering constraints. The parameters of this optimized design are then used as the reference design of the detailed conceptual design study. This is in fact a continuous process, with each conceptual fusion power plant design study leading to better models of many of the subsystems for use in the next generation of system optimization studies.

For an entire pure fusion power plant, the parameters of most interest include the following three system parameters:

(1) the overall system thermodynamic efficiency defined as:

$$\eta_{SYST} = \frac{P_{E(NET)}}{P_{NUC(TOT)}} = \frac{P_{E(BL)} + P_{E(DCS)} - P_{E(CIRC)}}{P_N M_N + P_\alpha}$$

where $P_{E(BL)}$ is the electric power generated from the blanket thermal power, $P_{E(DCS)}$ is the electric power generated from the mirror leakage power to the Direct Converter Subsystem (DCS) including its portion of the thermal bottoming plant, P_N is the fusion neutron power released, M_N is the blanket multiplication of the neutron power and P_α is the fusion alpha power released. $P_{E(CIRC)}$ is the power which must be recirculated to drive injectors and/or other plasma heating systems and any auxiliary systems.

(2) the specific capital cost of the power plant:

$$SCC_{TOT} \equiv \frac{C_{CAP}}{P_{E(NET)}} = \frac{C_{NI} + C_{BOP} + C_{DCS}}{P_{E(BL)} + P_{E(DCS)} - P_{E(CIRC)}}$$

where the total capital cost, C_{CAP}, consists of C_{NI}, the fusion reactor "nuclear island" costs; C_{BOP}, the cost of the balance of the plant excluding the DC subsystem; and C_{DCS}, the cost of the DC Subsystem. (The basic elements of a typical DC Subsystem are shown in Fig. 1.)

(3) the specific cost of generating electricity in mills/kW-hr which can be written in the simplified form

$$SGC_{TOT} \equiv \frac{C_{TOT}}{P_{E(NET)}\ t_{PA}} = \frac{C_{CAP} + C_{FUEL} + C_{OP} + C_{MAINT}}{P_{E(NET)}\ t_{PA}}$$

where C_{TOT} consists of the usual items: the capital costs, C_{CAP}, fuel costs, C_{FUEL}, operating costs, C_{OP} and maintenance costs, C_{MAINT}, and where t_{PA} is the number of hours per year that the plant is available. Systems codes such as the one described in Ref. [4] can produce estimates of the above system parameters.

Appendix B - Efficiency Loss Equations for Multi-stage VBDC's

The selection of the collector stage voltages is assumed to have been optimized to yield the maximum direct power recovery for a specific ion loss-cone energy distribution. The distribution function for the reference MPR (Mirror Power Reactor) is shown by the solid curve in Fig. 5. An exponential approximation, shown by the dashed curve is:

$$f_I \equiv \frac{1}{I_{I(M)}} \frac{dI_I}{dW_I} = \left[\frac{1}{\overline{W}_I - W_{I(MIN)}}\right] \exp\left[-\frac{W_I - W_{I(MIN)}}{\overline{W}_I - W_{I(MIN)}}\right] \tag{B1}$$

The exponential approximation can be seen to be reasonable good for this particular loss-cone distribution. As mentioned previously, the minimum ion energy for this case was $W_{I(MIN)} = 100$ keV, while the average ion energy was $\overline{W}_I \simeq 168$ keV.

Also, it should be remembered that the shape of this distribution function has a direct impact on the attainable direct conversion efficiency of multi-stage VBDC's as well as SSDC's. The more narrow the distribution in energy, the higher will be the ion collection efficiency, all other things being equal.

The ideal collection efficiency for a multi-stage VBDC is given in general form in Ref. [5]. For a three-stage VBDC this can be written:

$$\begin{aligned}
\eta_{C(ID)} &= \frac{P_{C(ID)}}{P_{I(C1)}} \\
&= \frac{I_{I(C1)}}{P_{I(C1)}}\left[V_{C1(ID)}\int_{V_{C1(ID)}}^{V_{C2(ID)} } f_I dW + V_{C2(ID)}\int_{V_{C2(ID)}}^{V_{C3(ID)}} f_I dW + V_{C3(ID)}\int_{V_{C3(ID)}}^{\infty} f_I dW\right] \\
&= \frac{1}{P_{I(C1)}}\left[V_{C1(ID)} I_{G1(ID)} + V_{C2(ID)} I_{G2(ID)} + V_{C3(ID)} I_{G3(ID)}\right]
\end{aligned} \tag{B2}$$

where $V_{C1(ID)}$, $V_{C2(ID)}$ and $V_{C3(ID)}$ are the ideal collector stage voltages; $I_{G1(ID)}$, $I_{G3(ID)}$ and $I_{G3(ID)}$ are the ideal ion currents collected in each group or energy band; and $P_{I(C1)}$ and $I_{I(C1)}$ are the ion beam power and current incident at the entrance to the first collector C1.

For the reference three-stage VBDC the optimum ideal voltages were found to be

$$V_{C1(ID)} = 100 \ , \quad V_{C2(ID)} = 155 \ , \quad V_{C3(ID)} = 240 \text{ kV}$$

for the actual leakage distribution. It is relatively easy to differentiate Eq. (15) using the approximate exponential energy distribution to find the optimum collector voltages for maximum efficiency. For the particular distribution of Fig. 5, the approximate results for $V_{C2(ID)}$ and $V_{C3(ID)}$ are only 10 - 20% too low compared to the above values ($V_{C1(ID)}$ is still selected as W_{MIN}).

Ideally 53.4% of the ion current would be collected on stage C1, 31.2% on stage C2, and 15.4% on stage C3. (Use of the exponential approximation to the distribution function yields 55.5%, 31.7% and 12.8%, respectively, so we can conclude that the approximation is reasonably good for this specific case.)

The actual collector voltage must be reduced by a factor to account for finite expansion ratio and angle of incidence Losses (a) (see Section 3):

$$V_{Ci} = V_{Ci(ID)} \cos^2\alpha_o \left(1 - \frac{1}{ER_C}\right) \tag{B3}$$

The actual collection efficiency (with no other losses) would then be given by Eq. (B2) with the above voltages replacing the ideal voltages multiplying each integral (the integration limits stay the same).

The modification of Eq. (11) for $\Delta\eta'_{Ci}$ for each collector stage of a VBDC

is thus:

$$\Delta\eta'_{Ci} = \frac{I_{(Gi \text{ at } Ci)}}{I_{I(M)}} \left[\frac{\overline{W}_{Gi} - V_{Ci}}{\overline{W}_I}\right] \tag{B4}$$

$$\text{where } \overline{W}_{Gi} = \int_{V_{Ci(ID)}}^{V_{C(i+1)(ID)}} f_I \times WdW \tag{B5}$$

It should be noted that $I_{(Gi \text{ at } Ci)}$ is the actual ion current of Group i which finally reaches stage Ci. The total collection efficiency loss for an N stage VBDC is thus given by

$$\Delta\eta'_C = \sum_{Cl}^{CN} \Delta\eta'_{Ci} \tag{B6}$$

The interception Losses (b), (c) and (d) on each collector stage can be estimated from the dimensions and incidence angles of the collector plates and structure using the equations of Ref. [10]. We defined the following relation for the interception loss fraction of ion Group Gj on collector stage Ci:

$$f_{INT(Ci - Gj)} = [\Delta f_{INT(\alpha_o)} + \Delta f_{INT(SAI)} + \Delta f_{INT(ST)}]_{(Ci - Gj)} \tag{B7}$$

The corresponding efficiency loss is given by:

$$\Delta\eta'_{INT(Ci - Gj)} = f_{INT(Ci - Gj)} \frac{I_{Gj(ID)}}{I_{I(M)}} \times \left[\frac{I_{(Gj \text{ at } Ci)}}{I_{Gj(ID)}}\right] \left[\frac{V_{Cj} - V_{Ci}}{\overline{W}_I}\right] \tag{B8}$$

The current ratio is given by:

$$\frac{I_{(Gj \text{ at } Ci)}}{I_{Gj(ID)}} = (1-f_{CXL})(1-f_{INT(GG)})(1-f_{INT(NG)}) \prod_{k=1}^{i-1} (1-f_{INT(Ck - Gj)}) \tag{B9}$$

The interception Loss (b) can be approximated as follows for small angles of incidence α_o and α_i:

$$\Delta f_{INT(\alpha_o)(Ci - Gj)} \approx \left\{ \frac{L_i}{H_i} \left| \frac{\alpha_o}{\sqrt{1 - \frac{V_{Ci}}{\bar{W}_{Gj} \cos^2 \alpha_o}}} - \alpha_i \right| + \frac{\delta_i}{H_i} \right\} \tag{B10}$$

L_i, H_i, δ_i and α_i are the collector plate length, spacing, orientation angle and thickness, respectively, for stage Ci. The additional interception Loss (c) due to the spread in the angle of incidence is very complex to calculate as shown in Ref. [10]. A rough scaling law for this loss is of the form [11]:

$$\Delta f_{INT(SAI)(Ci - Gj)} \approx \left[\frac{K_{SAI}}{(ER)_{GG}} \eta_{C(ID)} \right] (Ci - Gj) \tag{B11}$$

where K_{SAI} can be estimated from the angle of the cone of the ion velocity vectors. For the three-stage VBDC we have estimated an average value of $K_{SAI} \approx 10$ for all stages and ion groups.

The additional interception Losses (d) on the structural support members, $\Delta f_{INT(ST)}$, are very design dependent, and hence, no general equations can be given.

The direct power loss due to ion Group Gi interception on suppressor grid SGi is very small since V_{SGi} is typically only a few kV's less positive than V_{Ci}. The interception losses from other ion groups on SGi are assumed to be negligible since the suppressor grids are usually placed in the "shadow" of the collector plates. If this shadowing is not effective, the equations can easily be modified to include the additional interception and secondary emission losses.

The secondary emission Loss (e) due to ion interception of Group Gi by the suppressor grids SGi behind each collector plate of stage Ci (except the last one) can be estimated from:

$$\Delta\eta_{SEC(SGi-Gi)} = f_{INT(SGi-Gi)} \left(\frac{I_{Gi(ID)}}{T_{I(M)}} \right) \left(\frac{I_{(Gi \text{ at } SGi)}}{T_{Gi(ID)}} \right) \gamma_{SEC(SGi-Gi)} \left[\frac{V_{C(i+1)} - V_{SGi}}{\bar{W}_I} \right] \tag{B12}$$

where $\left(\frac{I_{(Gi \text{ at } SGi)}}{I_{Gi(ID)}}\right) = \left(\frac{I_{(Gi \text{ at } Ci)}}{I_{Gi(ID)}}\right) \left(1 - f_{INT(Ci - Gi)}\right)$ (B13)

This efficiency loss equation assumes that all the secondary electrons emitted from SGi go to the collector stage C(i + 1) just downstream of the suppressor grid.

Appendix C - Evaluation of the Thermal Power from the DC to the Bottoming Plant

For the SSDC as well as the VBDC reference designs, it has been decided to recover the thermal energy associated with the charge exchanged deuterium and tritium particles which impact on the expander walls. This can be done by placing a set of helium-cooled thermal panels in the form of chevrons on the entire expander wall (in front of the cryopanel assemblies on that portion of the expander wall where the cryopanels are located; see Fig. 8). These thermal panels would run at roughly 1000 K. The reason for adding thermal panels to the SSDC design is to see if this is cost effective when the charge exchange losses are allowed to be much larger than 1%.

The intercepted ion power plus the appreciable electron power (about 7.8% in these designs) collected by the grounded grids would also be transferred to the bottoming plant in both designs. This is accomplished by helium-cooling the 1 cm diameter grounded grid tubes.

The only thermal power not transferred to the bottoming plant in the present SSDC design is that due to the ion interception on the negative grids. It was decided to water-cool these 2 mm diameter wires by running very high pressure cold water through 1 mm holes in the wires. The resultant low temperatures completely eliminate the thermionic emission loss which would have resulted from the high incident ion flux at the negative grid (nominally 250 W/cm^2 in the reference design.)

For the SSDC with water-cooled negative grids, the equation for $f_{TH(BOTT)}$ becomes:

$$f_{TH(BOTT)} = 1 - \frac{P_{TH(NG)}}{P_{TH(TOT)}}$$

Thus $$f_{TH(BOTT)} = 1 - \left[\frac{(1 - f_e)(1 - f_{CXL})(1 - f_{INT(GG)})f_{INT(NG)}}{(1 - \eta_{SSDC})}\right] \quad (C1)$$

This has an average value of about 0.985 for the design parameters of the SSDC (for f_{CXL} in the range from 1 to 10%).

If it is decided to dispense with the thermal panels, and hence to absorb the charge exchange thermal power on low-temperature water-cooled panels, the expression for the fraction of the thermal power which goes to the bottoming plant becomes the following:

$$f_{TH(BOTT)} = 1 - \left[\frac{(1 - f_e)[f_{CXL} + (1 - f_{CXL})(1 - f_{INT(GG)})f_{INT(NG)}]}{(1 - \eta_{SSDC})}\right] \quad (C2)$$

For the three-stage VBDC, all thermal power from the negative grid and the first two collector stages is radiated either to helium-cooled thermal panels on the expander wall or to the helium-cooled third stage. Consequently $f_{TH(BOTT)}$ for this design is 1.0.

Appendix D - Discussion of Component Cost Equations

D.1 Burleigh-Type Vacuum Tank

The vacuum tank costing is based on a tank design by R. Burleigh which employs large fan-shaped concave membranes which are stressed by the external atmospheric pressure and are almost in pure tension (see Appendix E, Fig. E-1). These are edge-supported by large rings and a substantial edge structure. Based on Burleigh's reference design, the approximate equation for the weight given in Table 3A was developed.

For the reference design of the 3-stage VBDC, an expansion ratio, ER_{GG} = 400 was specified yielding a tank radius of about 50 m and a tank height of about 25 m. A desired charge exchange loss of only 1% (f_{CXL} = .01) was also specified somewhat arbitrarily. In order to achieve the low background density of neutral D_2 and T_2 gas required to meet this goal, Burleigh designed a tank with $\Theta_T = 180^o$. This yielded an expander wall surface area available for cryopanels of over 9000 m^2, which was just about enough to meet the 1% charge exchange loss requirement. (Most of the end area of the tank behind the direct converter modules was assumed to be unusable for cryopanels due to the neutron flux which leaks out the mirror exit and impinges on that surface.) Subsequent refinements of the cryopanel area requirements indicate that close to 12,100 m^2 may be required to achieve only 1% charge exchange loss in this design. However, the 9000 m^2 available on the expander walls comes very close, yielding only about 1.3% loss.

Based on the approximate equation for the total surface area, A_T, for a tank of this complex geometry given in Table 3B, a vacuum tank of this design for the three-stage VBDC would have a total inner surface area of about 13,100 m^2. The weight equation in Table 3B yields a total weight of about 1.04×10^7 kg;

this implies an average tank wall thickness of about 10 cm. For an installed cost of a stainless steel tank of \$13.2/kg [18], this vacuum tank would cost about \$135 x 10^6. This approach is referred to as Option A in the remainder of this paper. (The key characteristics of the various Options and Cases discussed in this paper are summarized in Table 4.)

D.2 Cryogenic Vacuum Pumping System

The cost of the cryogenic pumping system for handling the large quantity of D_2 and T_2 gas produced in each direct converter will be charged entirely to the DC subsystem. The cryo-pumping system consists of cryopanel assemblies, a liquid nitrogen refrigerator and a liquid helium refrigerator.

The components of the cryopanel assemblies are illustrated in Fig. 8. The required cryopanel area is given by the equation in Table 3A. The cost equation can be written as follows for a specific design:

$$C_{CP} = \tilde{C}_{CP} \left(\frac{K_{CP}}{f_{CXL}} \right)$$

where K_{CP} is about 121 m^2 for the VBDC design and about 12.3 m^2 for the SSDC design (with thermal panels assumed in front of the cryopanel assembly). The additional cost of the auxiliary vacuum pumping equipment necessary to remove the D_2 and T_2 gas evolved during the periodic defrosting of the cryopanels has not been evaluated in this study.

A simple approximation for estimating the average charge exchange cross-section based on the data in Ref. [11] is:

$$\bar{\sigma}_{CX} \approx 1.0 \times 10^{-19} \; e^{\frac{-\bar{W}_I}{63.3}} \quad (m^2)$$

The cryo-refrigeration cost equation of Table 3A is based on the cost

data of Ref. [19]. A linear fit to the efficiency data of Fig. 1 of this reference was made to obtain a simpler cost equation; the linear fit is accurate to about ± 15% from a refrigeration capacity, $\dot{Q}_{TOT}$, of 10 W to 10^7 W (which is less than the scatter in his data), and yields the relatively simple equation of Table 3A with the constants given in Table 3B.

For the cryopanel assembly and emissivities shown in Fig. 8, the total radiative plus convective heat flux to the liquid nitrogen panels behind the liquid helium panels and to the liquid-nitrogen-cooled chevrons in front of them has been estimated as about 0.325 kW/m^2 of frontal area. The corresponding total heat flux to the liquid-helium-cooled panels is estimated as 0.49 W/m^2, almost three orders of magnitude less than to the liquid-nitrogen-cooled surfaces.

The simplified cost equation for a specific design can be written:

$$C_{CR} = K_{CR} A_{CP}^{0.605}$$

where K_{CR} is about 1.72×10^5 for the liquid nitrogen refrigerator and about 3.15×10^4 for the liquid helium refrigerator for these specific cryopanel assemblies, emissivities, heat loads, etc. It can be seen from these numerical values that the liquid nitrogen refrigerator bears the brunt of the heat load in this design and costs about 5.5 times the liquid helium refrigerator. This suggests that it may be possible to reduce the total cryo-refrigeration costs by appropriate changes in various emissivities.

For 1% charge exchange loss, the costs of the three major components of the cryogenic vacuum pumping system for the VBDC design were proportioned approximately as follows: 54% for the cryopanels, 39% for the liquid nitrogen refrigerator, and 7% for the liquid helium refrigerator. For the smaller cryopanel area requirements of the SSDC design, the costs were proportioned approximately as follows for 1% charge exchange loss: 36% for the cryopanels, 54%

for the liquid nitrogen refrigerator and 10% for the liquid helium refrigerator.

It should be noted that the vacuum equipment to pump the small amount of helium produced by the fusion reactions has not been evaluated in this study.

D.3 Direct Converter Modules

The costing of the direct converter modules is based on the design of R. Werner in Ref. [5] shown in Fig. 3. The major cost item in a module of this type is the stainless steel stage; which dominates the cost of all the other elements and is estimated to be about 84% of the total module cost for the VBDC. The radiatively-cooled graphite first and second stages of the three-stage VBDC design are estimated to be less than 8% of the cost. A single VBDC module is about 2.5 m by 2.5 m by about 5 m long and is estimated to cost about $25,000 giving a cost of about $4000/m^2 of frontal area. As a first approximation, the SSDC is assumed to have about the same cost per unit frontal area.

D.4 DC Power Conditioning Equipment

In Ref. [7], the power conditioning costs to handle the direct current output from the direct converter and to invert it to AC power were estimated at about $40/kW$_e$ ($26/kW$_{th}$ of ion beam power) in 1972 dollars. For these present calculations the average value used was increased to $46/kW$_e$ estimated in 1975 dollars.

D.5 Thermal Panels

Gaseous helium-cooled thermal panels running at a nominal temperature of 1000 K were originally conceived as radiation receivers for the radiation-cooled graphite first and second stages of the three-stage VBDC. The thermal panels are chevron-shaped stainless steel assemblies placed over the entire inner surface of the expander wall (and of course, in front of the cryopanel assemblies wherever they are located). They are not needed on the end wall behind the DC

modules since negligible radiative power reaches that surface.

In trade off studies on the optimum charge exchange loss described in Section 6.3, it was found that values of f_{CXL} on the order of 10% are probably desirable for lower cryo-system costs. The thermal panels thus also serve to absorb any of the thermal power flow due to the charge exchange neutrals which impinge on the expander walls, and transfer this heat to the bottoming plant. For this reason, thermal panels were included not only in the VBDC design, but were also added to the reference SSDC design.

D.6 Thermal Bottoming Plant

The bottoming plant is assumed to be a modern steam powerplant with an effective thermal efficiency, $\eta_{TH(EFF)} \approx 40\%$. It may actually be part of the same steam powerplant which converts the blanket thermal energy to electrical power. For a plant with a steam generator heated by helium, an estimated cost of \$175/kW_e was assumed, based on the detailed study of Ref. [20]. The helium circulators are assumed to be included in this cost.

Appendix E - Direct Converter Vacuum Tanks

The present design envisions a large, fan-shaped vacuum tank enclosing each direct converter. These vacuum tanks are designed to withstand the full one atmosphere external pressure load. The design concept involves the use of concave stainless steel sheets in tension for the two main surfaces of the fan-shaped tanks. The pressure load is then taken by two large edge rings around the perimeter of the tension sheets. The two sheet sides are held apart by a stiffened edge structure of beams, auxiliary rings and cover panels placed between the two rings. This concept, designed by R. Burleigh for our application results in a near-minimum-weight structure and hence in a relatively low cost vacuum tank.

A sketch of Burleigh's vacuum tank design for the reference three-stage VBDC (with an expansion ratio to the grounded grid, $ER_{GG} = 400$) is shown in Fig. E-1. It consists of large top and bottom sheets which are concave sections of a sphere of 81 m radius. They are designed to be in essentially pure tension under the external atmospheric pressure load. Large edge rings and beams carry the atmospheric pressure load on the spherical sheets to end abutments (not shown in the figure).

Burleigh left only a half-dozen pages of rough hand calculations to document his design. These will be reproduced below (with some editing and relatively minor changes for better clarity and consistency) in order to provide a more permanent documentation of this novel, light-weight vacuum tank design.

The reference dimensions for these sample calculations have been adjusted to fit the final VBDC design:

R_T = 50.0 m (Burleigh R_T was 44 m)

H_T = 25.4 m (Burleigh H_T was 25 m)

θ_T = 180° (Same as Burleigh)

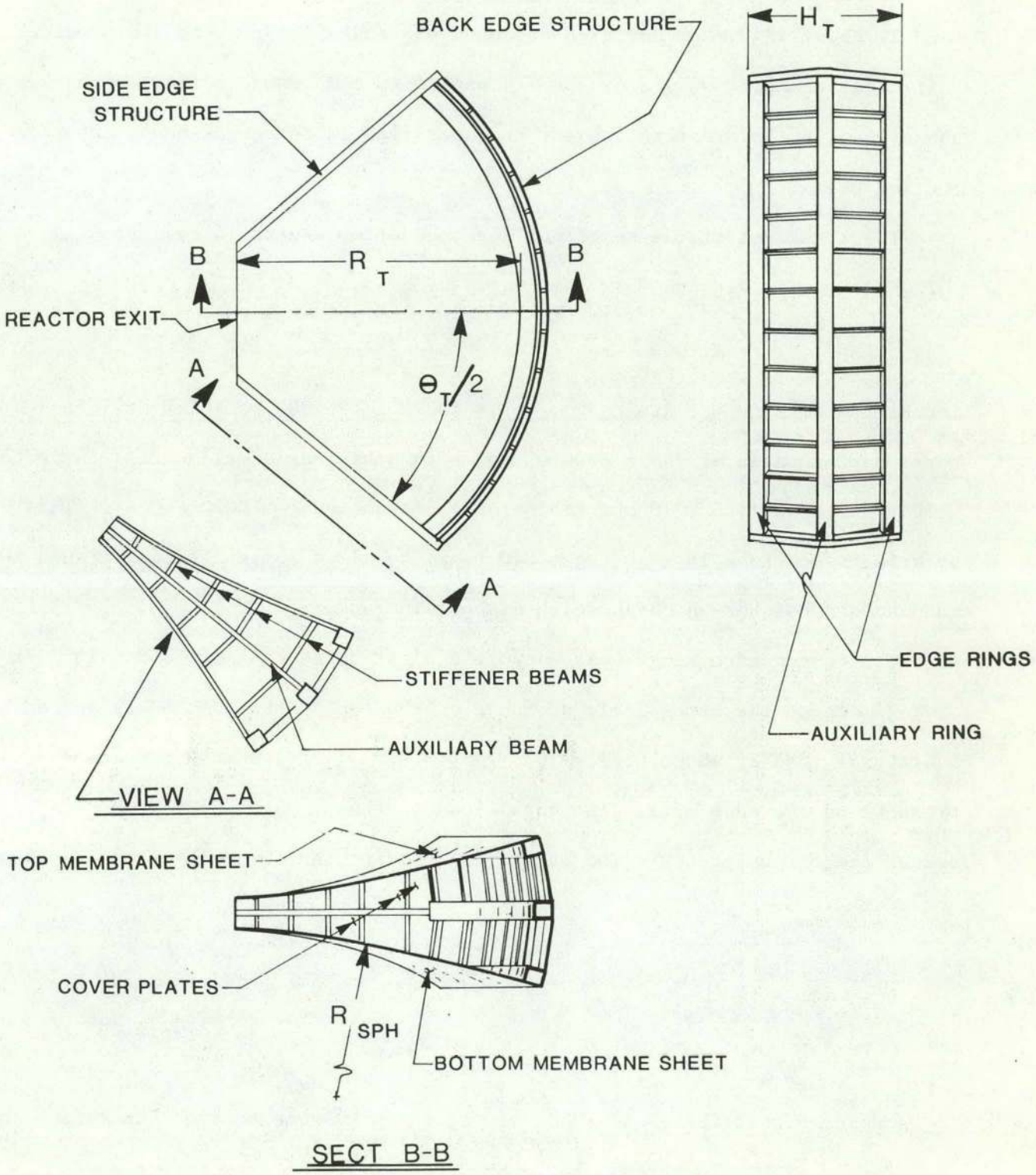

Fig. E-1 Geometry and nomenclature used in describing the Burleigh-type vacuum tank.

The actual B field expansion ratio to the back of the tank is about 617 (compared to $ER_{GG} = 400$ to the grounded grid). The B field fan angle at the back of the tank is about 124°, but Burleigh designed his tank for $\Theta_T = 180°$ to provide a sufficient expander wall area for cryopanels to pump down to very low background gas pressures (in order to achieve the specified 1% charge exchange loss from the ion beam).

The thickness of the spherical top and bottom sheets is estimated as:

$$t_{Sph} \sim \frac{R_{Sph}\, p}{2\sigma_{Allow}} \simeq 3.0 \text{ cm}$$

for $R_{Sph} = 81$ m, $p = 1$ atm and $\sigma_{Allow} = 138$ MPa (20,000 psi) for stainless steel. For a surface area of about 6900 m^2 for both stainless steel sheets, their total weight is about 1.66×10^6 kg (1826 tons), (assuming $\rho \simeq 8020$ kg/m^3). This has been increased to 2.56×10^6 kg (2820 tons) to allow for stiffening around the many access hatches which Burleigh did not include.

The curved edge rings must support a distributed load of 2.68×10^5 N/m (180,000 lb/ft) due to the atmospheric pressure on the top and bottom sheets and an additional load of about 6.71×10^4 N/m (45,000 lb /ft) due to the atmospheric pressure on the edge area. The total load is thus $S_E \simeq 3.35 \times 10^5 \frac{N}{m}$ around the circumference. The end forces holding the rings in place are thus:

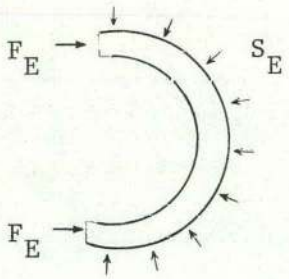

$$F_E = R_T\, S_E \simeq 1.68 \times 10^7 \text{ N} \quad (3.77 \times 10^6 \text{ lb})$$

It is assumed that these end loads are taken up by some sort of concrete abutments.

For an allowable stress of 138 MPa, the weight of each edge ring is:

$$W_{ER} = \rho\pi R_T\, A_{ER} = \rho\pi R_T \frac{F_E}{\sigma_{Allow}}$$

$$\simeq 1.53 \times 10^6 \text{ kg (1680 tons)}$$

where the ring cross-sectional area required is $A_{ER} \simeq 1.22\ m^2$.

Burleigh estimated the weight of the edge cover plates by simply assuming an average thickness of about 7.6 cm (3.0 inches). (It is not clear from his notes whether this includes an allowance for access hatches to permit removal of the DC modules.) Using his thickness estimate, the weight of the edge cover plates is:

$$W_{ECP} \simeq \rho \pi R_T H_T t_{ECP}$$

$$\simeq 2.39 \times 10^6 \text{ kg } (\sim 2630 \text{ tons})$$

He then estimated the weight of the edge stiffener beams as follows. The beams were assumed to be spaced 3.0 m apart around the circumference and curved outward 2 m at the center. Each beam is loaded axially by the edge rings and has an additional distributed load of 1 atm along its length. The axial force is estimated from

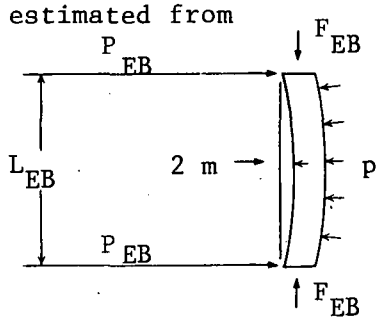

$$F_{EB} \simeq \frac{1}{2} \pi R_T^2 \, p \times \frac{1}{N_{EB}}$$

There appears to be a numerical error in Burleigh's original estimate of only 35 edge beams, N_{EB}. If we consider only the beams around the curved back edge structure, N_{EB} should be about 52 for $R_T = 50$ m. Then $F_{EB} \simeq 4.62 \times 10^6$ N (520 tons). These end forces create a moment at the beam center of about 1.85×10^7 N-m.

An opposing moment on the edge beams tending to straighten them out is produced by the distributed atmospheric load. At the beam center:

$$M_C = P_{EB} \, L_{EB} \Big/ 4 = pw \, L_{EB}^2 \Big/ 8$$

where w is the spacing between beams (3.0 m). Assuming $L_{EB} \simeq H_T$ we get $M_C = 2.41 \times 10^7$ N-m. The net moment requires a beam thickness calculated from:

$$M_{NET} = \sigma_{Allow} \left(\frac{I}{y} \right)_{EFF}$$

Including the edge cover plates as part of an effective T beam, Burleigh estimated a beam thickness of about 5.1 cm (2") for a beam depth of 1.52 m (5').

The weight of each edge beam is thus

$$W_{1EB} = \rho \, L_{EB} \, d_{EB} \, t_{EB}$$

$$\simeq 1.55 \times 10^4 \text{ kg (17.1 tons)}$$

For 52 edge beams, the total weight is 0.81×10^6 kg (about 890 tons).

The auxiliary edge ring weight was estimated very roughly by Burleigh to be about 1.82×10^5 kg (200 tons).

The weight of the entire side edge structure was only guessed at by Burleigh; he assumed a weight of 9.1×10^5 kg (1000 tons). This seems somewhat too low considering that we probably require extensive access hatches for replacement of cryopanel assemblies when necessary. Consequently, the side edge structure weight estimate has been increased to 1.36×10^6 kg (about 1500 tons).

The total reference Burleigh tank weight used in my scaling law is composed of the following component weights:

Spherical sheets: (with hatch stiffeners)	2.56×10^6 kg	(2820 tons)
Back edge main and auxiliary rings:	3.24×10^6 kg	(3560 tons)
Back edge cover plates:	2.39×10^6 kg	(2630 tons)
Back edge stiffener beams:	0.81×10^6 kg	(890 tons)
Total side edge structure:	1.36×10^6 kg	(1500 tons)
Total ref BT weight:	10.36×10^6 kg	(11,400 tons)

The Burleigh tank weight scaling law which I developed attempts to model these component weights in a simplified manner.

$$W_{BT} \simeq K_{BT} R_T^3 \left[\left(\frac{H_T}{R_T} \right)^{1.4} \left(\frac{\theta_T}{360} + 0.32 \right) + 0.21 \left(\frac{\theta_T}{360} \right) \right]$$

The first term models the entire back edge and side edge structure while the last term models the spherical top and bottom sheets including the allowance for extensive stiffening around access hatches.

For $K_{BT} = 196.4$ and the reference tank dimensions, this equation yields:

$$W_{BT} = 7.63 \times 10^6 \text{ kg} + 2.58 \times 10^6 \text{ kg}$$
$$= 10.21 \times 10^6 \text{ kg} \quad (11{,}230 \text{ tons})$$

This is within 1.5% of the more detailed estimate, and consequently, considered adequate for these preliminary cost estimates. Assuming \$13.2/kg installed cost for this type of stainless steel structure, the reference tank cost is about $\$135 \times 10^6$. This is shown on Fig. E-2 at $ER_{GG} = 400$. Plotted on this figure are the Burleigh-type tank cost trends predicted by this simplified scaling law and the expander wall area available for cryopanels.

Also shown on Fig. E-2 are estimates of the cost and expander wall area for a thin membrane tank with $\theta_{TT} = \theta_{BFF}$, the natural B field fan angle, and with an average tank wall thickness of only 1 cm. The curves of Fig. E-2 have been used to estimate the tank costs and expander wall area for Option A (the Burleigh-type vacuum tank) and Option B (the thin membrane tank). It has been assumed that these estimates are sufficiently accurate for both the VBDC's and the SSDC's with their much smaller expansion ratios.

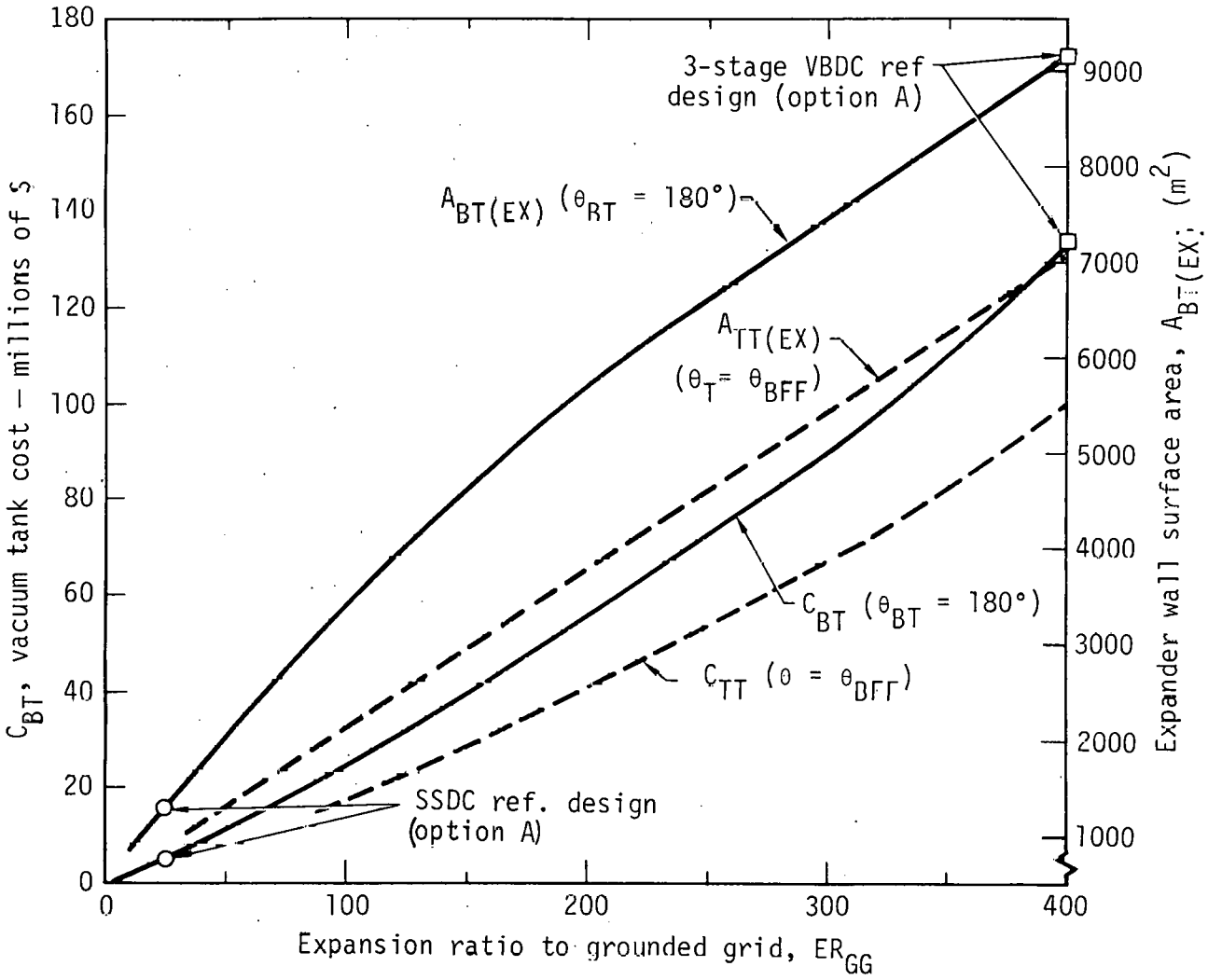

Fig. E-2 Tank costs and expander wall area available for cryopanels for the Burleigh tank and for a thin-walled tank for the reference direct converter designs.

Appendix F - Effect of Mirror Leakage Power Flux on DC Subsystem Costs

As an additional set of comparisons, it is interesting to see how the SCC's vary with the total mirror leakage power and the mirror leakage power flux defined as

$$q''_{(TOT)M} \equiv \frac{P_{(TOT)M}}{A_M}$$

These effects will be illustrated by two examples.

For the first example, we will compare the Possible Substitute SSDC (Case SS-IIPS) with the reference SSDC design of Case SS-IIB which handles 278 MW of mirror leakage power (at a mirror power flux of 53 MW/m^2) and requires an expansion ratio of 25, one quarter of the values of the Possible Substitute SSDC. We note that the specific capital cost of the SSDC of Case SS-IIB is about $\$146/kW_e$. It is slightly higher than the $\$135/kW_e$ of Case SS-IIPS. This is due to the fact that the electric power output for Case SS-IIPS is slightly more than four times that of Case SS-IIB (due to slightly higher efficiency) while the total DC Subsystem costs are only about 3.8 times that of Case SS-IIB. This seems to indicate that higher mirror leakage power flux should lead to lower SCC's, all other constraints being equal.

It should be noted that the dimensions and spacings of some of the grid and collector elements of the direct converter modules would have to be changed to handle the much higher ion power flux of Case SS-IIPS.

For the second example, we wish to compare the best VBDC for 10% charge exchange loss (Case VB-IIB) with a hypothetical VBDC (Case VB-IIH) which handles about 4 times the leakage power through the same mirror exit giving a mirror leakage power flux of 848 MW/m^2. This hypothetical situation is illustrated in Fig. F-1 where it is imagined that four times the leakage power (4448 MW)

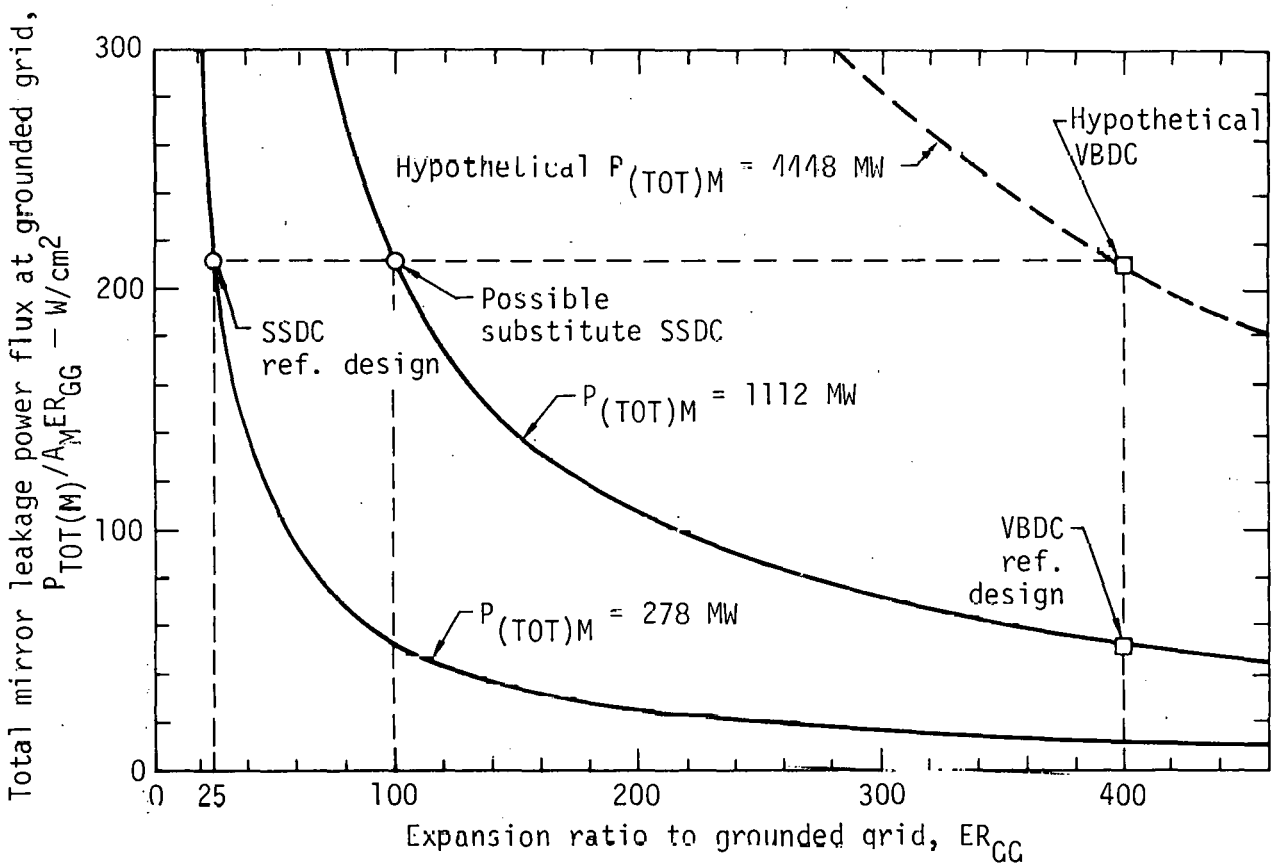

Fig. F-1 Comparison of the total leakage power flux at the mirror exit for several cases referred to in this study.

leaves the same mirror exit area using the same magnetic field coils and goes to the same VBDC at the same expansion ratio of 400.

This hypothetical VBDC would then operate not only at the minimum expansion ratio for acceptable ion trajectory distortion losses due to the residual B field, but also simultaneously at the maximum ion flux limit of about 250 W/cm^2 at the negative grid. This is clearly close to the highest power density possible for this three-stage VBDC design and should lead to the lowest specific capital costs. Figure 12 shows that this is indeed true; the SCC of the total VBDC Subsystem is only about $\$108/kW_e$ for the hypothetical Case VB-IIH compared to $\$156/kW_e$ for Case VB-IIB. However, it sould be cautioned that no way is known to create the plasma in the reference Yin Yang magnetic coils which would produce this large hypothetical leakage power.

NOTICE

This report was prepared as an account of work sponsored by the United States Government. Neither the United States nor the United States Energy Research & Development Administration, nor any of their employees, nor any of their contractors, subcontractors, or their employees, makes any warranty, express or implied, or assumes any legal liability or responsibility for the accuracy, completeness or usefulness of any information, apparatus, product or process disclosed, or represents that its use would not infringe privately-owned rights.

NOTICE

Reference to a company or product name does not imply approval or recommendation of the product by the University of California or the U.S. Energy Research & Development Administration to the exclusion of others that may be suitable.

Printed in the United States of America
Available from
National Technical Information Service
U.S. Department of Commerce
5285 Port Royal Road
Springfield, VA 22161
Price: Printed Copy $; Microfiche $3.00

Page Range	Domestic Price	Page Range	Domestic Price
001–025	$ 3.50	326–350	10.00
026–050	4.00	351–375	10.50
051–075	4.50	376–400	10.75
076–100	5.00	401–425	11.00
101–125	5.50	426–450	11.75
126–150	6.00	451–475	12.00
151–175	6.75	476–500	12.50
176–200	7.50	501–525	12.75
201–225	7.75	526–550	13.00
226–250	8.00	551–575	13.50
251–275	9.00	576–600	13.75
276–300	9.25	601–up	*
301–325	9.75		

*Add $2.50 for each additional 100 page increment from 601 to 1,000 pages; add $4.50 for each additional 100 page increment over 1,000 pages.

Technical Information Department
LAWRENCE LIVERMORE LABORATORY
University of California | Livermore, California | 94550